Published on www.elsevier.com/locate/geomorph

Geomorphology 253 (2016) 508–523

http://dx.doi.org/10.1016/j.geomorph.2015.10.030

# The application of landslide sampling strategies using a grid-based bi-variate statistical susceptibility model

(1) Haydar Y. Hussin, (2) Veronica Zumpano, (3) Paola Reichenbach, (4) Simone Sterlacchini, (2) Mihai Micu, (1) Cees van Westen, (2) Dan Bălteanu

(1) Faculty of Geo-Information Science and Earth Observation (ITC), University of Twente, 7500 AE, Enschede, The Netherlands
(2) Institute of Geography, Romanian Academy, 12 Dimitrie Racovita, 023993, Bucharest, Romania
(3) Consigilio Nazionale delle Ricerche, Instituto di Ricerca per la Protezione Idrogeologica (CNR-IRPI), Perugia, Italy
(4) National Research Council of Italy, Institute for the Dynamic of Environmental Processes (CNR-IDPA), Piazza della Scienza, 1, 20126 Milano, Italy

Corresponding author: Haydar Y. Hussin, e-mail: h.y.hussin@utwente.nl, Tel.number: +31644752633

## Abstract

This study had three aims. The first aim was to assess the flexibility and applicability of the Weights-of-Evidence (WofE) landslide susceptibility model in areas that are very different in terms of size, geo-environmental settings and landslide types. The second aim was to study how grid-based landslide sampling strategies effect the overall performance of the WofE susceptibility model. The final aim was to test the sensitivity of the WofE method to changes in the landslide sample size used to train the model. This is in order to understand whether there is a minimum number of landslides required for a sufficient susceptibility performance. Two case study areas were chosen for this study: the Fella River Basin (Eastern Italian Alps) containing debris flows and the Buzau County (Romanian Carpathians) with shallow landslides. The WofE model was overall able to predict debris flow scarps as well as shallow landslides, despite the Buzau County being four times larger, with lower quality data. The three landslide sampling strategies used were: (1) the landslide scarp centroid, (2) points populating the scarp on a 50m grid and (3) the entire scarp polygon. The areas (AUC) under the success (SRC) and prediction rate curve (PRC) were used to assess model performance and validation respectively. The highest success rates were obtained when sampling shallow landslides as 50m grid-points and debris flow scarps as polygons. Prediction rates were highest when using the entire scarp polygon method for both landslide types. A sample size of 104 debris flow scarps were sufficient to predict the remaining 941 debris flows in the Fella River Basin, while 161 shallow landslides was the minimum required number to predict the remaining 1451 scarps in the Buzau County. Below these landslide sample thresholds, model performance was too low. However, using more landslides then the threshold produced a “plateau effect” with little to no increase in the model performance rates. We further found that several of the landslide susceptibility maps produced with different strategies and sample sizes had similar model performance rates but produced spatially different maps. A spatial agreement analysis is recommended as a follow up to assess how the maps can be combined to obtain an optimal result for future decision-makers in both study areas.

# 1. Introduction

The spatial prediction of landslides in the form of susceptibility assessment studies have been applied now for the past 40 years with new techniques continuously being developed and updated. An overwhelming amount of literature has been published on the different methods that have been used throughout the years. The extensive guidelines, reviews and overviews related to landslide hazard and risk (Varnes et al., 1984; Soeters and van Westen, 1996; van Westen et al., 1997; Aleotti and Chowdhury, 1999; Guzzetti et al., 1999; Van Westen, 2000; Dai et al., 2002; Crozier and Glade, 2005; Glade and Crozier, 2005; Wang et al., 2005; Fell et al., 2008; van Westen et al., 2008; Corominas et al., 2013) generally divide landslide susceptibility methods into qualitative (e.g. heuristic, geomorphological analysis, expert based index/weighting) or (semi-) quantitative approaches (e.g. statistical and deterministic analysis). The quantitative approaches and, specifically, the statistically-based susceptibility assessments are widely applied methods in the field of landslide hazard and risk for mapping scales ranging between 1:25,000 and 1:50,000 (van Westen et al., 2006; van Westen et al., 2008). These statistical methods follow a single important assumption, that slope instability factors causing landslides in the past will statistically determine the spatial probability of landslide occurrence in the future (Soeters and van Westen, 1996). According to this assumption, the predictive capability of statistical susceptibility methods rely on two input data: the inventory of past landslide events and the landslide causative factor maps (also called “landslide predisposing” factors, “landslide conditional” factors or “slope instability” factors). The way in which landslides are represented and sampled in a GIS determines how the causative factor information is extracted for susceptibility mapping and is therefore a very important aspect in landslide hazard zonation studies.

Landslides are generally mapped using vector-based data, which are represented by points (Brenning, 2005; Galli et al., 2008), polygons (van Westen et al., 2000; Chung and Fabbri, 2005) and lines (Donati and Turrini, 2002). In some cases, slope failures can be directly mapped as raster data, for example by semi-automated mapping from remote-sensing imagery (Brenning, 2009; Mondini et al., 2011). The mapping representation is determined by the type and availability of data, the spatial scale of the analysis, the purpose of the study and the mapping methods used, among others (Soeters and van Westen, 1996; Guzzetti et al., 1999; van Westen, 2004; Glade and Crozier, 2005; van Westen et al., 2008). All statistical landslide susceptibility zonations require the selection of mapping units, which are the subdivisions that make up the susceptibility map. A variety of mapping units are reported in the literature (Guzzetti et al., 1999; Van Den Eeckhaut et al., 2009). The choice of the mapping unit is crucial, because it determines how landslides will be sampled to prepare the training and prediction (validation) subsets for the susceptibility modeling that can be vector-based (Carrara et al., 1995; Guzzetti et al., 2005; Galli et al., 2008) or grid-based (Carrara, 1983; van Westen, 1993; Chung and Fabbri, 1999; Remondo et al., 2003).

In grid-based (also referred to as pixel or raster-based) susceptibility assessments, landslide mapping representations are either overlaid in their original format (e.g. points, polygons) on grid-cell causative factor maps to directly extract data from the factor maps or are converted to a raster map and then used for data extraction. The pixel size is determined by the spatial resolution of the susceptibility analysis (Lee et al., 2004; Tian et al., 2008; Legorreta Paulin et al., 2010; Catani et al., 2013) which is also scale and data dependent. According to the literature concerning grid-based landslide susceptibility mapping, four general methods are used to sample landslide pixels (Fig. 1):

**(1)** The landslide is sampled as a single pixel (Atkinson and Massari, 1998; Lee et al., 2002; Van Den Eeckhaut et al., 2006; Thiery et al., 2007; Yilmaz, 2010; von Ruette et al., 2011; Piacentini et al., 2012). Usually, the pixel is the centroid of the entire landslide or of the scarp area. The single pixel can be selected to represent the "top-point" of a landslide placed by an expert on the initiation area, which is not necessarily the centroid (Qi et al., 2010; Gorum et al., 2011; Xu et al., 2013). The single pixel is often applied if landslides have been mapped directly as points or if the landslides in polygon format are not reliable for the susceptibility analysis (e.g. data scarcity, size of the area, scale related issues, etc.). Pixels located within the landslide boundary, but not assigned to the single/centroid point in some cases are considered as non-landslide pixels.

**(2)** All the pixels within the entire landslide body or the scarp area can be sampled as landslide pixels (Ayalew and Yamagishi, 2005; Poli and Sterlacchini, 2007; Blahut et al., 2010; Ozdemir, 2011; Sterlacchini et al., 2011; Petschko et al., 2013; Regmi et al., 2013; Petschko et al., 2014). In this case, all pixels located outside the landslide polygons are considered as non-landslide areas.

**(3)** The "seed-cell" approach (Süzen and Doyuran, 2004; Nefeslioglu et al., 2008a; Nefeslioglu et al., 2008b; Yilmaz, 2010; Demir et al., 2013; San, 2014) selects pixels within a buffer polygon around the upper landslide scarp area and sometimes part of the flanks of the accumulation zone. The buffer distance which determines the number of cells representing the landslide is defined by an expert. The purpose of this method according to Süzen and Doyuran (2004) is to consider "that the best undisturbed morphological conditions (conditions before landslide occurrence) would be extracted from the vicinity of the landslide polygon itself". However, this could lead to problems in cases where landslide boundaries coincide with main morphological boundaries (e.g. top of the landslide at the crest of a ridge).

**(4)** The Main Scarp Upper Edge (MSUE) approach selects pixels on and around the landslide crown-line (Clerici, 2002; Donati and Turrini, 2002; Clerici et al., 2006; Jurko et al., 2006; Clerici et al., 2010; Capitani and Federici, 2013; Capitani et al., 2013), which basically is the upper edge of the landslide scarp area. The MSUE method was applied for the following reasons (Donati and Turrini, 2002; Clerici et al., 2006): the upper edge of the scarp area was the most identifiable feature in the landslide mapping, the entire depletion zone (scarp area) was less visible due to recovery of the slope and the scarp area was often partly covered by the accumulation zone making the boundary between the two zones difficult to identify. Similar to the seed-cell methodology, the MSUE method is able to represent the landslide using pixels in "undisturbed morphological conditions" by projecting an artificial crown-line at a certain distance from the original crown-line, with the distance and length assigned by the expert (Clerici et al., 2006).

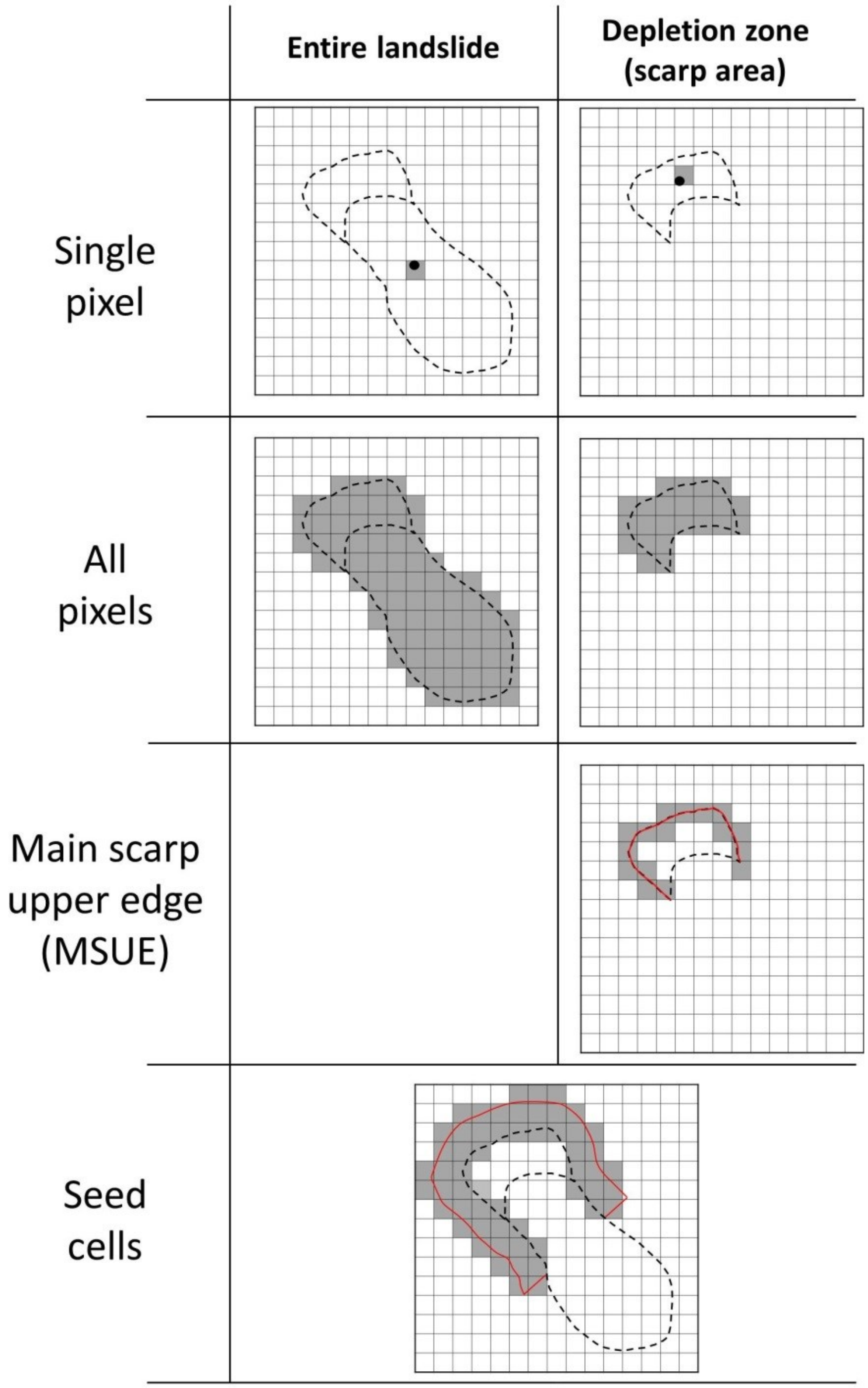


Fig. 1. Landslide grid-based sampling strategies exploited in susceptibility studies.

A number of studies have compared some of the sampling techniques regarding landslide susceptibility success and prediction. Poli and Sterlacchini (2007) studied the effect of landslide sampling using the landslide centroid and points populating the polygon every 50 and 20m. They found that one point every 50m within a landslide polygon performed better than representing the landslide using a single centroid and the 20m points. Yilmaz (2010) compared the susceptibility using the scarp polygon, seed cells and a single point. According to Yilmaz (2010), "validations of the obtained maps indicated that the more realistic results obtained from the analyses where the scarp sampling strategy was used, however, it was relatively similar with the seed cells strategy. It can be evaluated that the two strategies such as scarp and seed cells considered have relatively similar accuracy". The single point sampling had lower performance rates. Simon et al. (2013) compared the extraction of slope angle information between landslide polygons and their centroids. They concluded that using centroid points could have some disadvantages like abstracting landslide causative information not located at the actual initiation points, but located in less significant factor classes or even outside the actual polygon boundary due to using the point of gravity. In this paper we will specifically test and compare the first two methods mentioned above, with an addition of a variation on the second method of sampling within the entire scarp polygon.

Once the expert determines which grid-cells are considered landslide or stable non-landslide areas, sampling is required to define the number of pixels to train and validate the susceptibility model. The modeler needs to decide not only the number of landslide pixels but also the number of non-landslide pixels to be used in assessing the success and prediction capability of the model. The ratio between landslide and non-landslide areas depends among others on the type of statistical model used in the susceptibility assessment. As Heckmann et al. (2014) summarized for logistic regression and other types of regression analysis, the ratio often used ranges between 1:1 to 1:10. However, larger ratios have also been used (Melchiorre et al., 2008; Felicísimo et al., 2013; Heckmann et al., 2014), including in other types of statistical techniques like the Bayesian approaches where sometimes all the non-landslide pixels are applied in the analysis (Blahut et al., 2010; Regmi et al., 2010). Recent studies have been conducted to understand the effects of landslide sample size on susceptibility mapping and prediction (Hjort and Marmion, 2008; Heckmann et al., 2014; Petschko et al., 2014). Hjort and Marmion (2008) assessed the effect of the sample size on the susceptibility of geomorphological processes like permafrost and solifluction in an area of 600 $km^2$ using model resolutions of 1 and 25 hectares. They found that for a sufficient model performance, producing AUC values ranging between 0.80 and 0.95, 100 to 200 samples were required of a population of more than 1700 data points. Heckmann et al. (2014) sampled 1000 non-landslide subsets ranging the sample size from 50 to 5000 pixels of 5 m resolution in two small areas of 7 and 19 $km^2$, while sampling 81 landslide pixels. They recommended a minimum of 300-350 non-landslide pixels, corresponding to a ratio of 1:3.7 to 1:4.3 (81:300 – 81:350) and obtaining an average area under the ROC curve of 0.83. Petschko et al. (2014) applied a 1:1 ratio of landslide to non-landslide pixels of 5 m resolution in an area of 15850 $km^2$ and found that as the sample size increased from 50 to 12562 pixels (total number of landslides), so did the AUC of the ROC curve increase from 0.76 to 0.84, with a slight plateauing at 3200 pixels or 25% of the landslide inventory. The literature indicates that there is no ideal fixed percentage or ratio for landslide and non-landslide sample sizes, and is further dependent on the statistical technique used in the susceptibility analysis.

Most of the research analyzing the effects of landslide sampling strategies and landslide sample sizes on susceptibility mapping have either used regression analysis techniques (e.g. logistic, linear, multivariate regression, etc.) or machine learning methods (e.g. artificial neural networks, generalized boosting method, etc.). Furthermore, these sensitivity analyses were conducted in single case study areas and mainly using single landslide types. In this paper we applied the widely used Bayesian bi-variate Weights-of-Evidence (WofE) susceptibility model to carry out two types of assessments. The first assessment is testing susceptibility success and prediction using three different landslide sampling strategies: (1) the centroid scarp point, (2) points located every 50 m within the scarp polygon and using (3) the entire scarp polygon. The second assessment is a sensitivity analysis of the WofE susceptibility mapping using different landslide sample sizes. In order to study the applicability and flexibility of our study, we applied our assessments to two completely different case study areas in terms of size, geo-environmental settings and most importantly different landslide types, namely debris flows and shallow landslides. The aim is to understand how sensitive the Weights-of-Evidence model is to our two tests, to find which landslide sampling strategy is best suitable for each case study area and landslide type, and to determine the minimum number of landslides needed in each area for sufficient susceptibility success and prediction results.

## 3. Case study areas

In this paper we selected two study areas (Fig. 2) to test and compare the results of different landslide sampling techniques for the susceptibility modeling. The first area is the Fella River Basin located in the Eastern Italian Alps with a total size of approximately 760 $km^2$. The Fella River Basin lies in the province of Udine within the autonomous region of Friuli-Venezia-Giulia. The area borders Austria and Slovenia and is part of an important corridor for international travel and logistics, winter tourism and a gas-pipeline route. Land cover consists of predominately forested areas (75%), with approximately 10% bare surface and 8% grasslands, with the urban areas located along the valley bottoms and on alluvial fans (Malek et al., 2014). The geology is made up of Permian and Triassic rocks covered by quaternary deposits. The Permian rocks consist of the Bellerophon Unit with dolomite and black limestone, while the Triassic rocks are made of the Werfen formation with calcareous-marls and the Serla formation consisting of dolomite and dolomitic limestone (Calligaris et al., 2008). Quaternary deposits are found across the study area in the form of debris screes, glacial and alluvial deposits. The elevation ranges from 250 to 2750 m.a.s.l., with a mean slope value of 33°. The multiple systems of monoclines, bends and faulting have caused extreme fracturing of bedrocks and outcropping of calcareous dolomitic sequences. This has led to the formation of very steep talus and scree slopes producing large amounts of debris stored within many secondary streams and debris flow channels flowing towards the Fella River. The latest major debris flow event occurred in August 2003 (Fig. 3), where approximately 1 million cubic meters of debris was triggered by an extreme rainfall event and deposited downslope at the bottom of the valleys. This event also was also the cause of a major flood of the Fella River (Tropeano et al., 2004). The area further regularly experiences shallow and deep seated landslides (Pasuto et al., 2000) and flash flooding (Creutin and Borga, 2003; Borga et al., 2007; Borga et al., 2008).

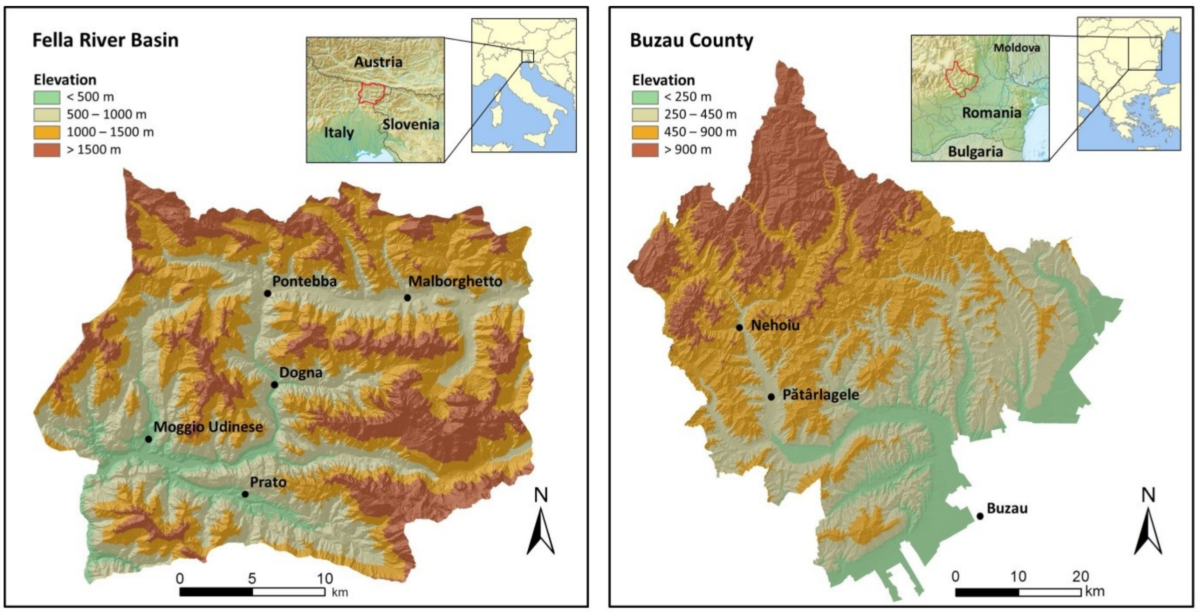


Fig. 2. Location and hill shaded relief maps. On the left the Fella River Basin (Friuli-Venezia-Giulia region, Italy) and on the right the Buzau County (Romania).

The second study area is the northern part of the Buzau County (Romanian Carpathians) that has a total area of 3230 km$^2$. The Buzau County consists partly of hilly and mountainous (Sub-Carpathians and Carpathians) areas, with the other half consisting of lower lying plains (Sarata-Buzau Plain). The county marks the southern half of the Vrancea seismic region, which represents the most seismically-active area of Romania and one of the most important in Central and South-Eastern Europe (Georgescu, 2002). The high-altitude north-western half outlines two parallel regions with different morphological process patterns. The internal part corresponds to the Buzau Carpathians, a low-to-mid altitude mountainous sector built on Cretaceous and Paleogene flysch, with packs of generally cohesive sandstones alternating with schistose sandstones and clayey-marly schists. The Carpathians, reaching a maximum elevation of 1300-1700 m, are generally conformable to the structural morphometry of rounded summits and ridges separated by large saddles or deeply-incised valleys (500-800 m relative relief). The slopes, usually covered (at least in the lower third) by relict landslide deposits, show inclinations of 15 to 45°. The external part is represented by the Buzau Sub-Carpathians, a low-to-high sector of alternating rounded hills and large depressions. The area contains less cohesive and heterogeneous Mio-Pliocene molasse deposits, with a mix of marls, clays, sands, gravels and large salt massifs and diapire folds, including small areas with loose schistose sandstones. The rounded hills extend from 250 to 900 m in altitude, while the dense river network is situated at 300-500 m. The slopes, intensely affected by active landslides (Fig. 3), have inclinations ranging from 10 to 30°. Landslide include numerous relict (and mostly dormant) landslide deposits, showing a high reactivation potential (Groapa Vântului landslide) and a number of active debris and rock slides featuring a high magnitude-low frequency pattern (Micu and Bălteanu, 2013). The Sub-Carpathian slopes are more frequently affected by medium and low magnitude mudflows and shallow-to-medium-seated translational and rotational earth and debris slides (Micu and Bălteanu, 2013).

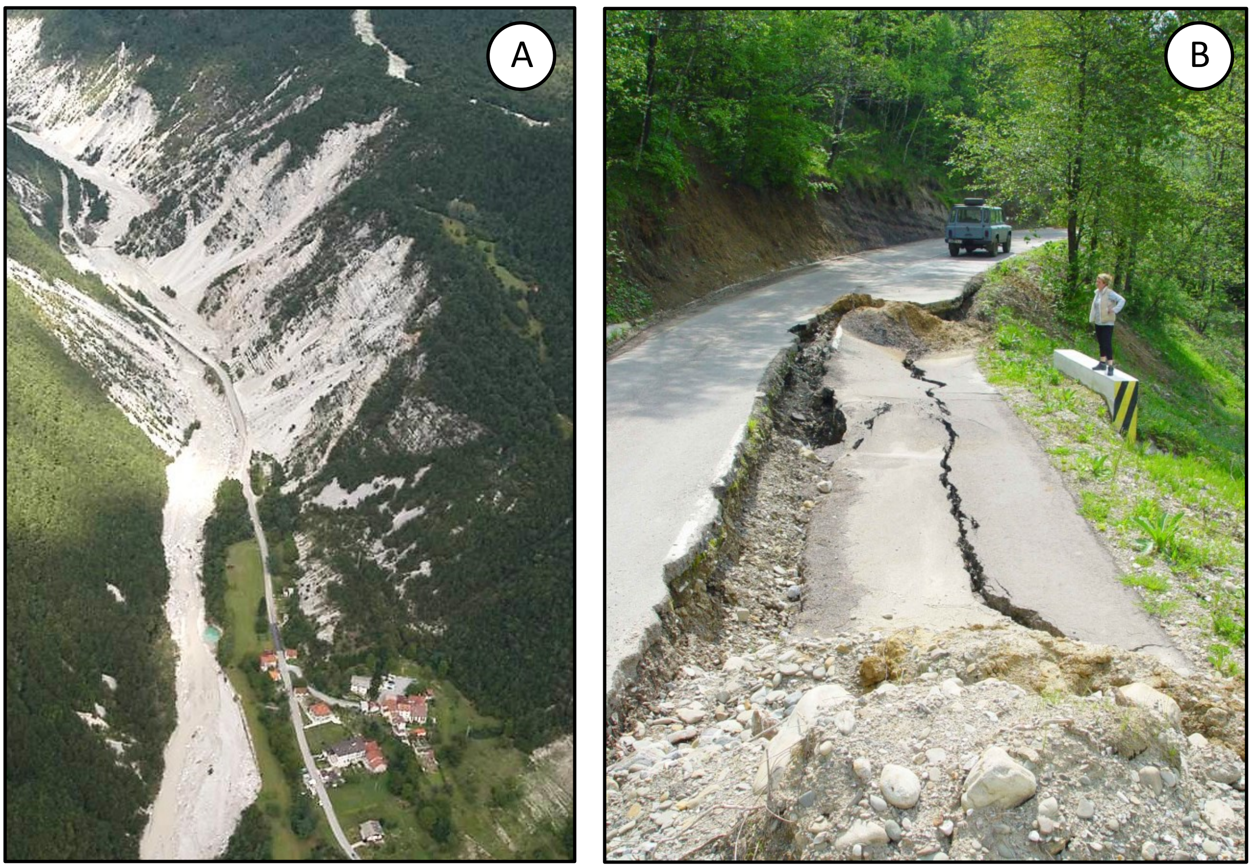


Fig. 3. (A) Major debris flow events that occurred in the Fella River Basin in 2003 and (B) an example of a shallow landslide in the Buzau County damaging a road.

### 3.1 Landslide inventories and thematic data

The historic debris flow inventory of the Fella River Basin (Fig. 4) was produced through the analysis of historic archives and interpretation of aerial and satellite imagery between 1999 and 2011 by the Italian Landslide AVI (CNR-IRPI, 2014) and IFFI projects (ISPRA, 2014), the Geological Service of the Friuli-Venezia Giulia region (FVG) and landslide experts at University of Trieste. The inventory consists of 1046 debris flow scarp area polygons, excluding the accumulation zone. The Buzau County contains 1612 mapped shallow landslide scarp areas (Fig. 4) from image interpretation of aerial orthophotos between 2005 and 2008 and integrated with information obtained from the Romanian Emergency Situation Inspectorate (ISU) and field observations.

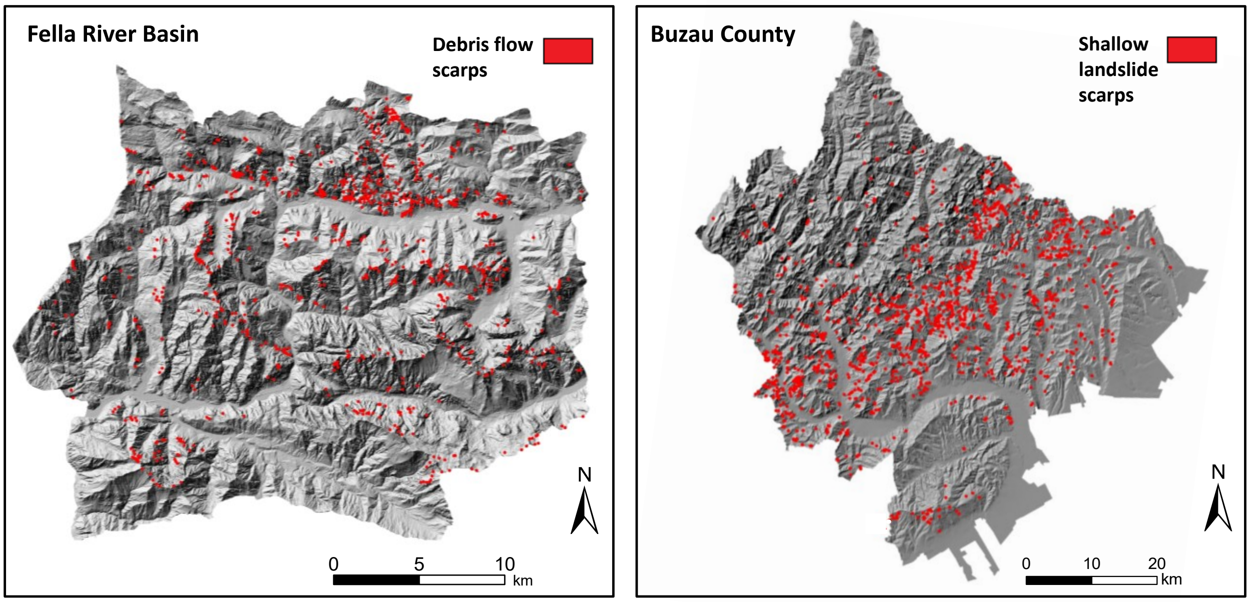


Fig. 4. Landslide inventory maps. On the left the debris flow scarps located in the Fella River basin and on the right the shallow landslide scarps in the Buzau County. The scarps are portrayed as centroid points.

The Digital Elevation Model (DEM) of the Fella River Basin was acquired from airborne laser scanning by the Civil Protection of the Friuli-Venezia Giulia region in 2003 (PC-FVG, 2014). The DEM has a pixel resolution of 20m, which is the pixel dimension we used for all the causative factor maps and the susceptibility zonation. According to a previous study (Hussin et al., 2013), 5 causative landslide factor maps (lithology, land-cover, altitude, plan curvature and slope) were used in the susceptibility analysis for debris flow initiation. The lithological map available at 1:150,000 scale was produced by the FVG Geological Service and originally contains more than 35 classes, which were reclassified in 8 classes. The land-cover map at 1:100,000 scale was developed by the CORINE land cover project (EEA, 2014) and later updated by the MOLAND project (JRC, 2014). The map with more than 30 classes was generalized to 7 classes based on similarities in land cover types. Both geo-environmental factor maps were rasterized using a 20m grid resolution. The three factors derived from the DEM were classified into 10 quantile classes. The quantile classification has been applied in several landslide susceptibility studies (Castellanos Abella et al., 2008; Blahut et al., 2010; Martha et al., 2013) and is useful to proportionately distribute rank-ordered data to better study the influence of factors on landslide occurrence.

The Buzau County DEM with a pixel resolution of 25m was derived from the contour-lines of a 1:25,000 scale topographic map produced in 1984. The 5 landslide causative factor maps (altitude, internal relief (m/ha), slope, land-cover and soil) used for the shallow landslide susceptibility analysis were derived from previous studies (Hussin et al., 2013; Zumpano et al., 2013; Zumpano et al., 2014). The three DEM derived factors were classified into 10 quantile classes. The land-cover map at 1:5,000 scale was derived from aerial photo interpretation (ANCPI, 2014) and contained 9 classes. The soil map at 1:200,000 scale is classified in 11 classes and was derived from the Soil Maps of Romania updated from 1963 to 1994 (ICPA, 2014). The soil map was used instead of the geology due to the nature of the shallow to medium seated landslides. Soil information was a better indicator of landslide initiation because it better represented the instable shallow material properties, while the lithological map represented the bedrock. Preliminary tests were carried out using the lithological map, resulting in poor prediction of landslides, which indicated that the lithological data available was much less significant than the soil data (Zumpano et al., 2014).

Table 1 summarizes the differences between the two case study areas. They are significantly different in terms of size, geology, morphology and landslide types. The Buzau County is more than 4 times larger than the Fella River area, but has a landslide (centroid) point density half of the Fella River Basin. The model pixel sizes are different due to the difference in the DEM resolution but the pixel dimensions (20 and 25m) can be considered similar and comparable for the purpose of the analysis.

Table 1 List of the thematic data and area statistics for the Fella River Basin and Buzau County.

| Information | Fella River Basin | Buzau County |
|---|---|---|
| Geo-environmental factors | Lithology<br>Land-cover | Soil map<br>Land-cover |
| DEM derived factors | Altitude<br>Plan curvature<br>Slope | Altitude<br>Internal relief<br>Slope |
| Landslide type | Debris flows | Shallow landslides |
| Study area size | 764.75 $km^2$ | 3230.57 $km^2$ |
| Landslide area | 7.25 $km^2$ | 9.76 $km^2$ |
| Pixel size | 20m | 25m |
| Total number of pixels | 1911883 | 5168940 |
| Number of landslide pixels | 18125 | 15551 |
| Number of landslides (centroid points) | 1046 | 1612 |
| Landslide (centroid) point density per $km^2$ | 1.368 | 0.499 |

## 5. Methodology

### 5.1 Weights-of-Evidence (WofE) susceptibility model

To prepare the landslide susceptibility maps, we applied the statistical Weights-of-Evidence (WofE) method in both study areas. The WofE technique was originally developed for quantitative mineral potential mapping to predict the location of possible gold deposits (Bonham-Carter et al., 1988; Bonham-Carter et al., 1989). However, it has been successfully applied in many landslide susceptibility assessments (van Westen, 1993; Lee et al., 2002; van Westen et al., 2003; Lee and Choi, 2004; Süzen and Doyuran, 2004; Neuhäuser and Terhorst, 2007; Thiery et al., 2007; Blahut et al., 2010; Regmi et al., 2010; Ozdemir and Altural, 2013) and is based on the assumption that factors causing landslides in the past will determine the spatial occurrence of future landslide initiation in areas currently free of landslides. A probabilistic Bayesian approach is applied to determine the conditional probability between the presence/absence of each causative factor and the presence/absence of a landslide. For every factor map (e.g. land-cover, lithology, etc.) a weighting table is produced that includes for each class (e.g. grassland, bare rock) the positive weight ($W^+$), which indicates the importance of the "presence" of this class on the occurrence of landslides. The table also has the negative weight ($W^-$) which evaluates the importance of the "absence" of the class on landslide occurrence and the contrast ($W^+$ - $W^-$). The contrast is considered a measure of the overall importance of a factor map class on the conditions causing landslide occurrence. The advantages of WofE are its quick and cost effective approach and the capability of combining the subjective choice of the classified factors by the expert with the objective data driven statistical analysis of the GIS. For details on the WofE methodology applied for landslide susceptibility the reader is referred to Lee et al. (2002).

The calculation of weight tables for each factor and the subsequent susceptibility mapping was carried out using the Weights-of-Evidence Arc-SDM (Spatial Data Modeller) (Sawatzky et al., 2009) geoprocessing tools in ArcGIS 10. and is a common main indicator used in Weights-of-Evidence landslide susceptibility assessments (Neuhäuser and Terhorst, 2007; Poli and Sterlacchini, 2007; Regmi et al., 2010; Schicker and Moon, 2012; Ozdemir and Altural, 2013). All susceptibility maps used for visualization and for spatial comparison were classified into 10 equal-area classes, which is a widely used method in classifying landslide susceptibility maps (Chung and Fabbri, 2003; Lee, 2005; Lee and Digna, 2005; Pradhan et al., 2008; Pradhan, 2011; Sterlacchini et al., 2011; Akgun, 2012; Papathanassiou et al., 2013; Chalkias et al., 2014; Galve et al., 2014). The relative probability values in the unclassified susceptibility maps were used to assess the model performance using Success Rate Curves (SRCs) (Chung and Fabbri, 1999; Chung and Fabbri, 2003). Prediction Rate Curves (PRCs) are then calculated to assess the predictive power of the susceptibility map by using a prediction landslide subset and are produced in the same way as the SRCs. The area under the curve (AUC), which is a value ranging between 0 and 1 or expressed as a percentage from 0 to 100%, is used as a final assessment of the SRCs and PRCs (Chung and Fabbri, 1999; Chung and Fabbri, 2003; Carrara et al., 2008; Blahut et al., 2010).

## 5.2 Landslide sampling strategies

The sampling strategies exploited to prepare susceptibility models in both test areas are summarized in Fig. 5. The vector-based representation from landslide mapping determines which pixels are identified as landslide scarp areas. Once the landslide and non-landslide pixels are determined, the pixels can be sampled to create the subsets for training the susceptibility model and to assess its predictive capability.

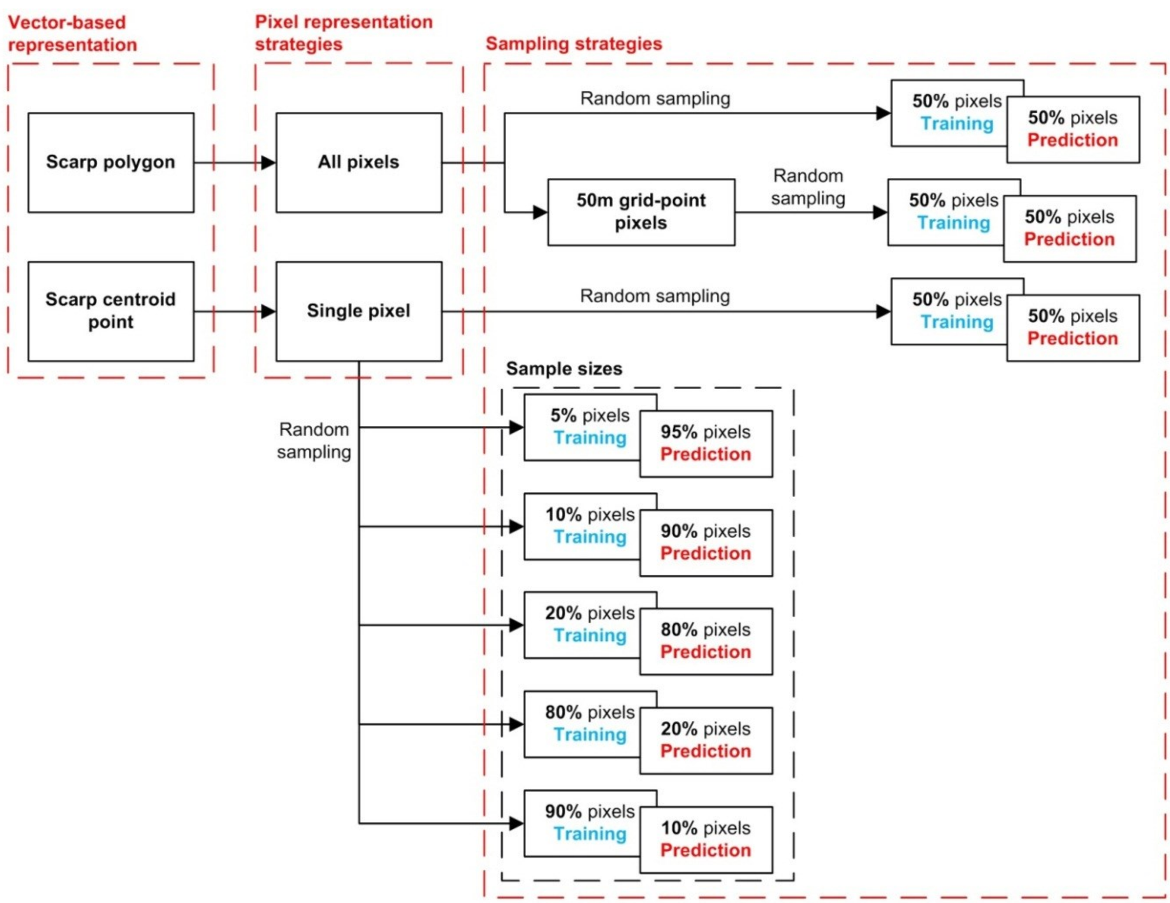


Fig. 5. Flow chart showing the use of landslide representation and sampling to prepare training and prediction subsets for the WofE susceptibility model

To test different sampling strategies, three types of pixel inventories were produced. The first test consisted of pixels corresponding to the scarp polygon centroid points. If the center of gravity of the polygon was located outside the scarp area, an ArcGIS operation was applied to force the centroid point to be located inside the polygon boundary. The second inventory consisted of pixels corresponding to points within the scarp polygon separated by a 50m grid. The third inventory contained all the pixels corresponding to the landslide scarp. The purpose of using the 50m grid-points was to have a landslide sample that populated the scarp polygon with a number of pixels more than a single centroid but less than using the entire polygon. Table 2 shows the number of pixels associated to each of the three sampling methods. The three inventories were randomly sampled into two subsets, with each subset containing 50% of the pixels. The first subset was used to train the susceptibility model to create the susceptibility map and produce the success rate curve (SRC). The second subset was applied to test how well the model was able to predict landslides, using the prediction rate curve (PRC).

Table 2 The total number of pixels used in the WofE susceptibility model in both study areas related to three different types of landslide pixel sampling methods

| Sampling methods | Buzau County Scarp pixels | Fella River Scarp pixels |
|---|---|---|
| Centroids | 1612 | 1046 |
| 50m grid-points | 2482 | 3472 |
| Scarp polygon | 15551 | 18125 |

The sensitivity of the WofE susceptibility model to landslide sample size was tested using the centroid sampling method. All the non-landslide (absence) pixels were considered in the sensitivity analysis. Different landslide (presence) pixel samples were separately random sampled from the centroid inventory of each study area. The 1046 debris flow scarp centroids of the Fella River Basin were separately random sampled into the following sizes: 31, 52, 104, 209, 523, 836, 941 and correspond respectively to 3, 5, 10, 20, 50, 80 and 90% of the inventory. The Buzau County 1612 shallow landslide centroids were randomly sampled into sample sizes of 80, 161, 322, 806, 1290, 1451, which also corresponded respectively to 5, 10, 20, 50, 80 and 90% of all shallow landslide centroids. These samples were used as training subsets but also as prediction subsets. For example, when 10% was randomly sampled for training, the remaining 90% was considered as a prediction subset. However, the same 90% was also used to train the model, while the same 10% was used for model prediction. Therefore, every sample size between 10 and 90% had one chance to be the training and prediction subset.

## 6. Results

Fig. 6 shows the WofE susceptibility model contrast values of the factor map classes for the different landslide sampling strategies. Bare rock areas in both case studies are a significant source of landslide scarps in terms of land cover. The lithology most contributing to debris flow sources in the Fella River basin is dolomite and limestone, while the soil types in the Buzau County having the most influence on shallow landslide scarps are the Aquisalids and Erodisols. Fig. 6 also indicates that in the Fella area, the presence of debris flow sources is generally more significant as the altitude, plan curvature and slope increase. In the Buzau County, shallow landslides are mainly focused in areas in the middle altitude and slope ranges.

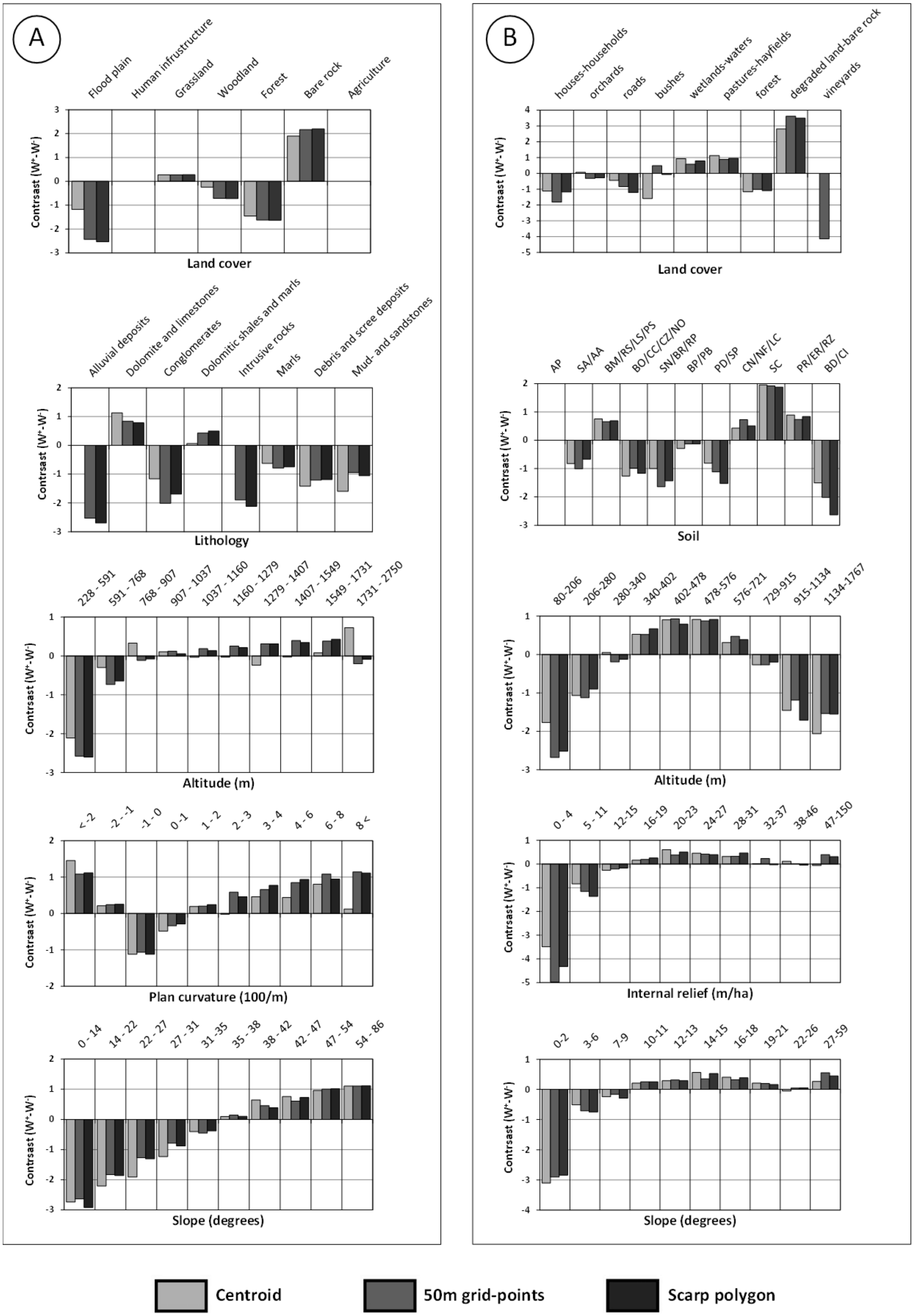

A
Flood plain
Human infrustructure
Grassland
Woodland
Forest
Bare rock
Agriculture
Contrsast (W⁺-W⁻)
Land cover
Alluvial deposits
Dolomite and limestones
Conglomerates
Dolomitic shales and marls
Intrusive rocks
Marls
Debris and scree deposits
Mud- and sandstones
Lithology
228 - 591
591 - 768
768 - 907
907 - 1037
1037 - 1160
1160 - 1279
1279 - 1407
1407 - 1549
1549 - 1731
1731 - 2750
Altitude (m)
< -2
-2 - -1
-1 - 0
0 -1
1 - 2
2 - 3
3 - 4
4 - 6
6 - 8
8 <
Plan curvature (100/m)
0 - 14
14 - 22
22 - 27
27 - 31
31 -35
35 - 38
38 - 42
42 - 47
47 - 54
54 - 86
Slope (degrees)
B
houses-households
orchards
roads
bushes
wetlands-waters
pastures-hayfields
forest
degraded land-bare rock
vineyards
Land cover
AP
SA/AA
BM/RS/LS/PS
BO/CC/CZ/NO
SN/BR/RP
BP/PB
PD/SP
CN/NF/LC
SC
PR/ER/RZ
BD/CI
Soil
80-206
206-280
280-340
340-402
402-478
478-576
576-721
729-915
915-1134
1134-1767
Altitude (m)
0 - 4
5 - 11
12-15
16-19
20-23
24-27
28-31
32-37
38-46
47-150
Internal relief (m/ha)
0-2
3-6
7-9
10-11
12-13
14-15
16-18
19-21
22-26
27-59
Slope (degrees)
Centroid
50m grid-points
Scarp polygon

Figure 6 Weights-of-Evidence contrast values ($W^+$ - $W^-$) of each factor map for the different sampling strategies in (A) the Fella River Basin and in (B) the Buzau County. The acronyms of the soil classes are taken from the Romanian System of Soil Taxonomy (RSST-2000, in Romanian) and translated according to the USDA Soil Taxonomy, 1999 (Florea and Munteanu, 2000): AA=Alluvial Protosoil; AP=Water; BD=Brown argilloilluvial soil; BM=Brown eu-mesobasic soil; BO= Brown acid soil; BP=Brown luvic soil (podzolite); BR=Brown-red soil; CC=Cambic chernozem; CI=Argilloilluvial chernozem; CN=Grey soil; CZ=Chernozem; ER=Erodisoil; LC=Hydromorphic soil; LS=Litosoil; NF= Black clinohydromorphic soil; NO=Black acid soil; PB=Brown iron-illuvial soil (podzol); PD=Podzol; PR=Pseudo Rendzine; PS=Psamosoils; RP=Brown-reddish luvic soils; RS=Regosol; RZ=Rendzina; SA=Alluvial soil; SC=Aquisalids; SN=Solonetzs; SP=Albic-luvic soil (argilloilluval podzol).

The Weights-of-Evidence contrast values related to the sample size sensitivity test are shown in in Fig. 7 and 8 for the Fella River Basin and Buzau County, respectively. The overall trend in contrast values between the factor classes is similar to Fig. 6. However, for each class within a factor map there can be different trends found when increasing the landslide training sample size for the susceptibility modeling. Fig. 7 shows that in the mud- and sandstone class of the lithology map, there is an increase in the negative contrast as the sample size increases, indicating that the more landslides are used to train the model, the less that mud- and sandstone has an effect on landslide occurrence. In some cases there is not a clear trend. Figure 7 shows a negative contrast of slope class 35-38° when using 52 scarp centroid pixels. This same class shifts to a positive contrast after using 104 landslide pixels to train the model. An opposite trend can be seen in certain altitude classes, where an increase in the sample size shifts the contrasts from positive to negative or lower values (Fig 7 and 8). This is possibly caused by a shift in distribution of landslide pixels to different altitude classes as the surface area representing the scarp polygon increases. The largest shifts in contrast values for the Fella River (Fig. 7) are found in the forest class of the land cover map, the 1037-1160 m class of the altitude map and the 31-35° class of the slope map. For the Buzau County (Fig. 8) the largest shifts are found in the altitude classes and the classes of the internal relief factor map.

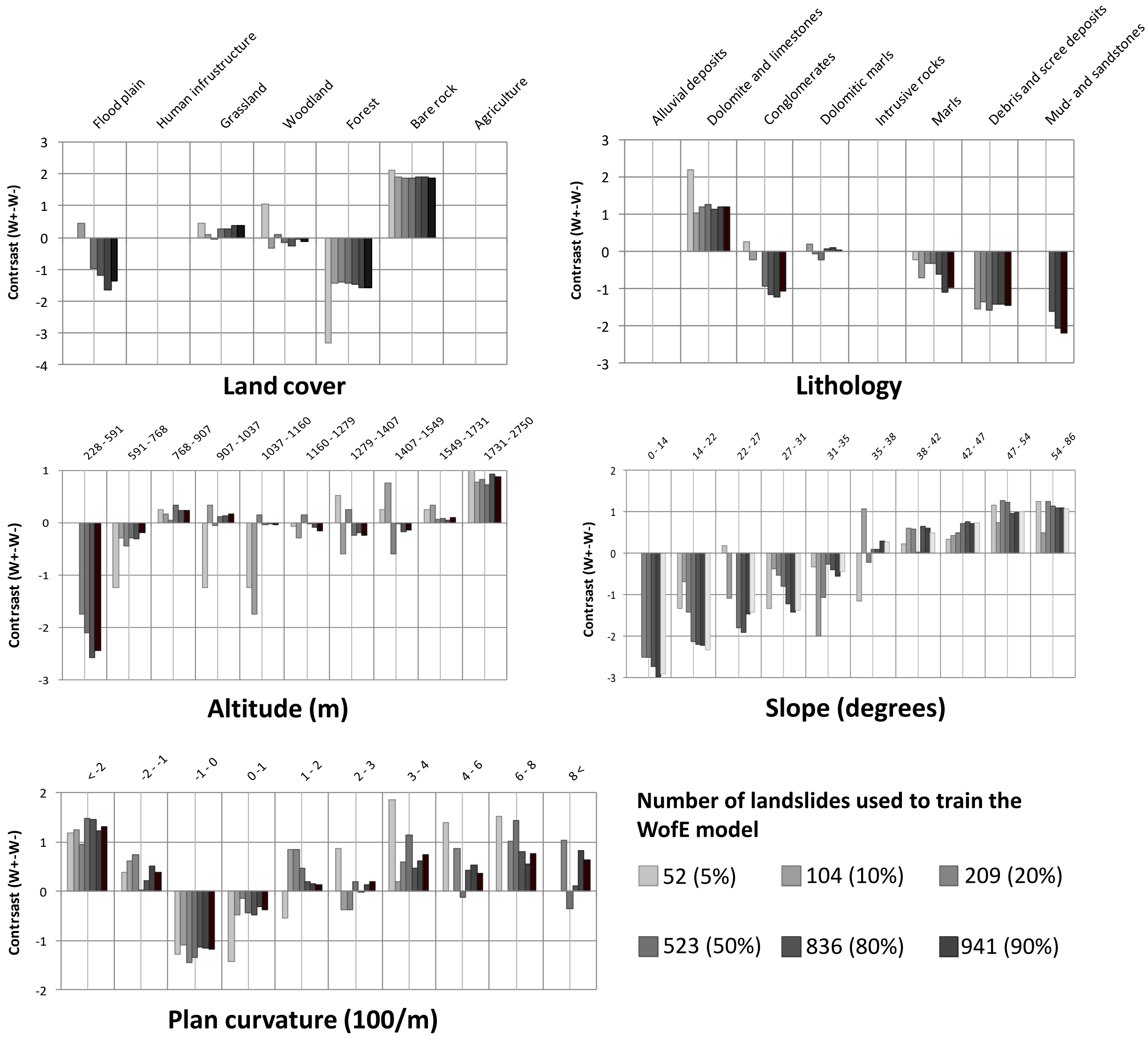


Figure 7 Weights-of-Evidence contrast values ($W^+ - W^-$) for each factor map applied in the susceptibility assessments using the different sample sizes in the Fella River Basin

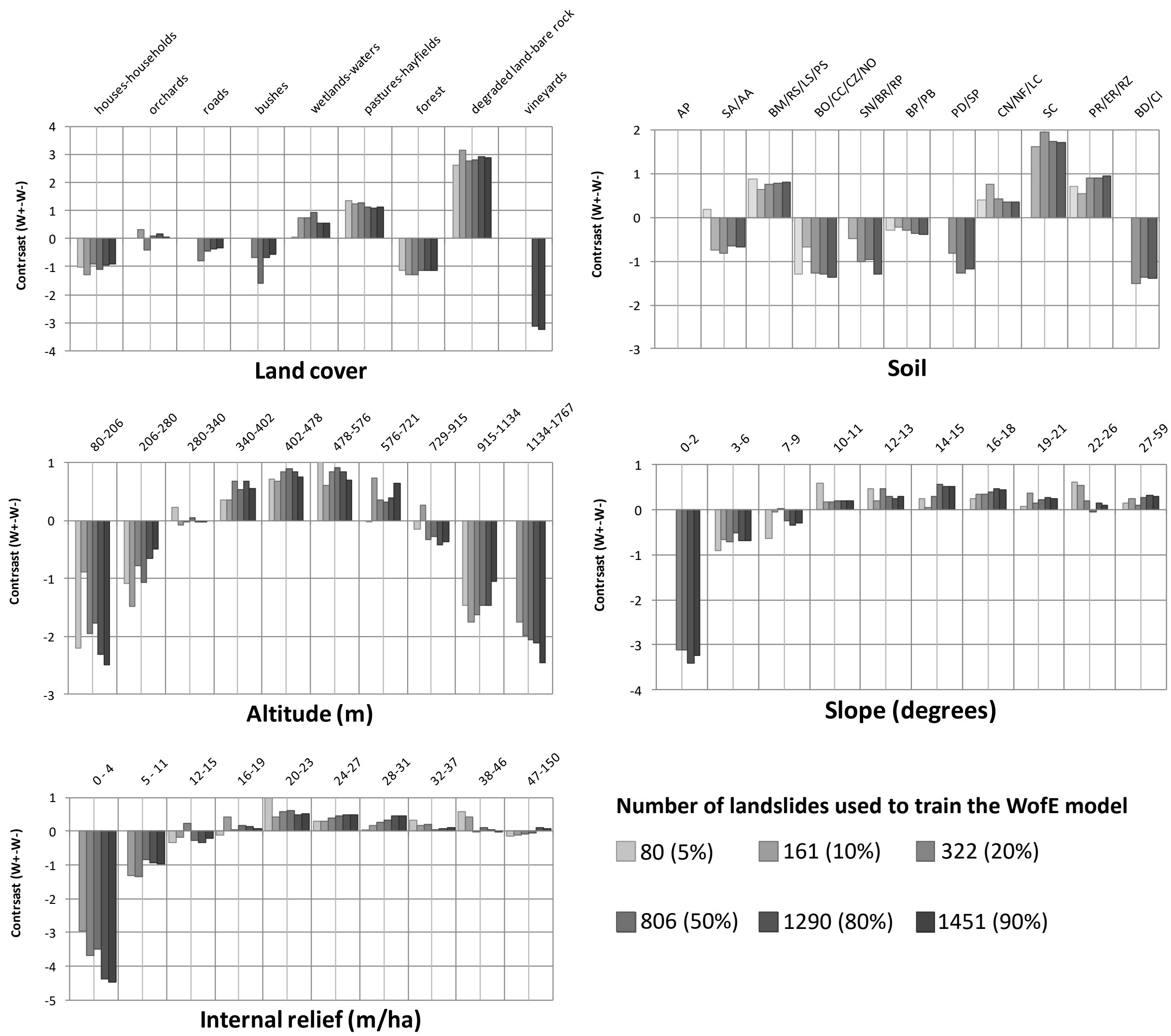


Figure 8 Weights-of-Evidence contrast values ($W^+$ - $W^-$) for each factor map applied in the susceptibility assessments using the different sample sizes in the Buzau County

The susceptibility maps that were produced using landslide centroid pixels and classified into 10 equal area classes are shown in Fig 9. For the Fella River Basin, the AUC values for the SRC and PRC were 82.53% and 81.26%, respectively. The Buzau County susceptibility map produced AUC values of 79.77% for the SRC and 79.49% for the PRC. The debris flow source susceptibility in the Fella River basin is higher at areas with high slope angles and where bare rocks are most persistent. Whereas the shallow landslide susceptibility in the Buzau County is higher in the middle altitude and slope angles and follows more or less the boundary between the Carpathians and lower Sub-Carpathians. These results also correspond well with the contrast values previously shown in Fig. 8.

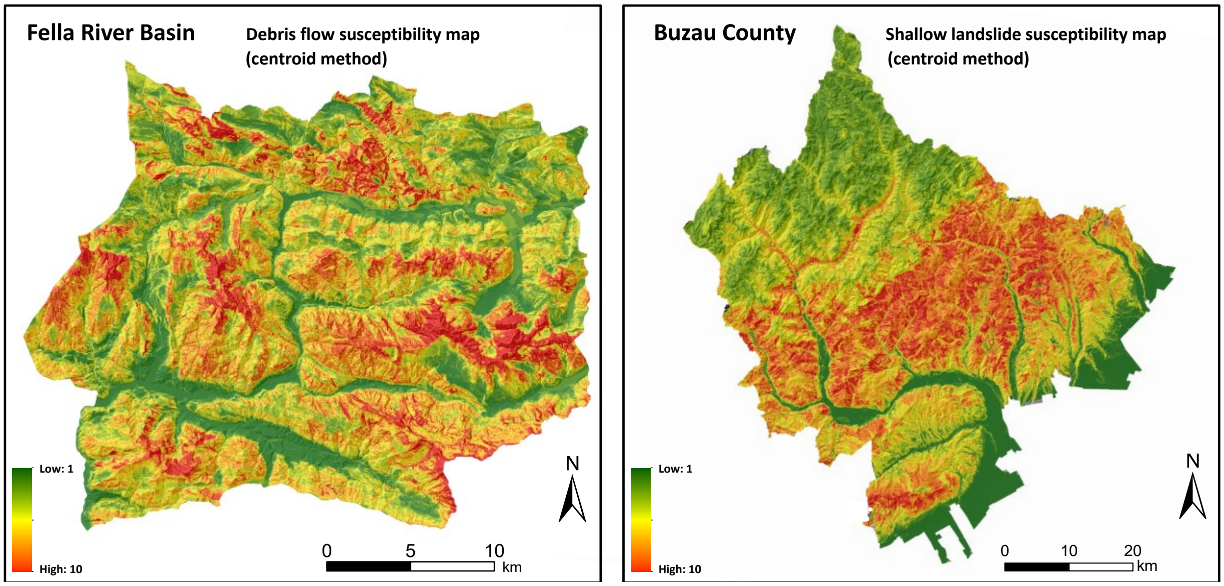


Figure 9 Best performing susceptibility maps modeled with landslide centroid pixels for (left) the Fella River Basin and (right) the Buzau County case study areas.

Figure 10 shows sections of the susceptibility maps for each of the three tested landslide sampling strategies. In both areas, there is a noticable increase in medium to high susceptibile areas when comparing the centroid method with the polygon strategy. The centroid method also seems to show different boundary conditions in the low to medium susceptibility classes compared to the other methods. In the Buzau county, there is a slightly stronger shift in susceptibility to higher classes going from centroid to 50m points. Overall, the Fella River has more changes in the susceptibility mapping with the different strategies than in the Buzau County.

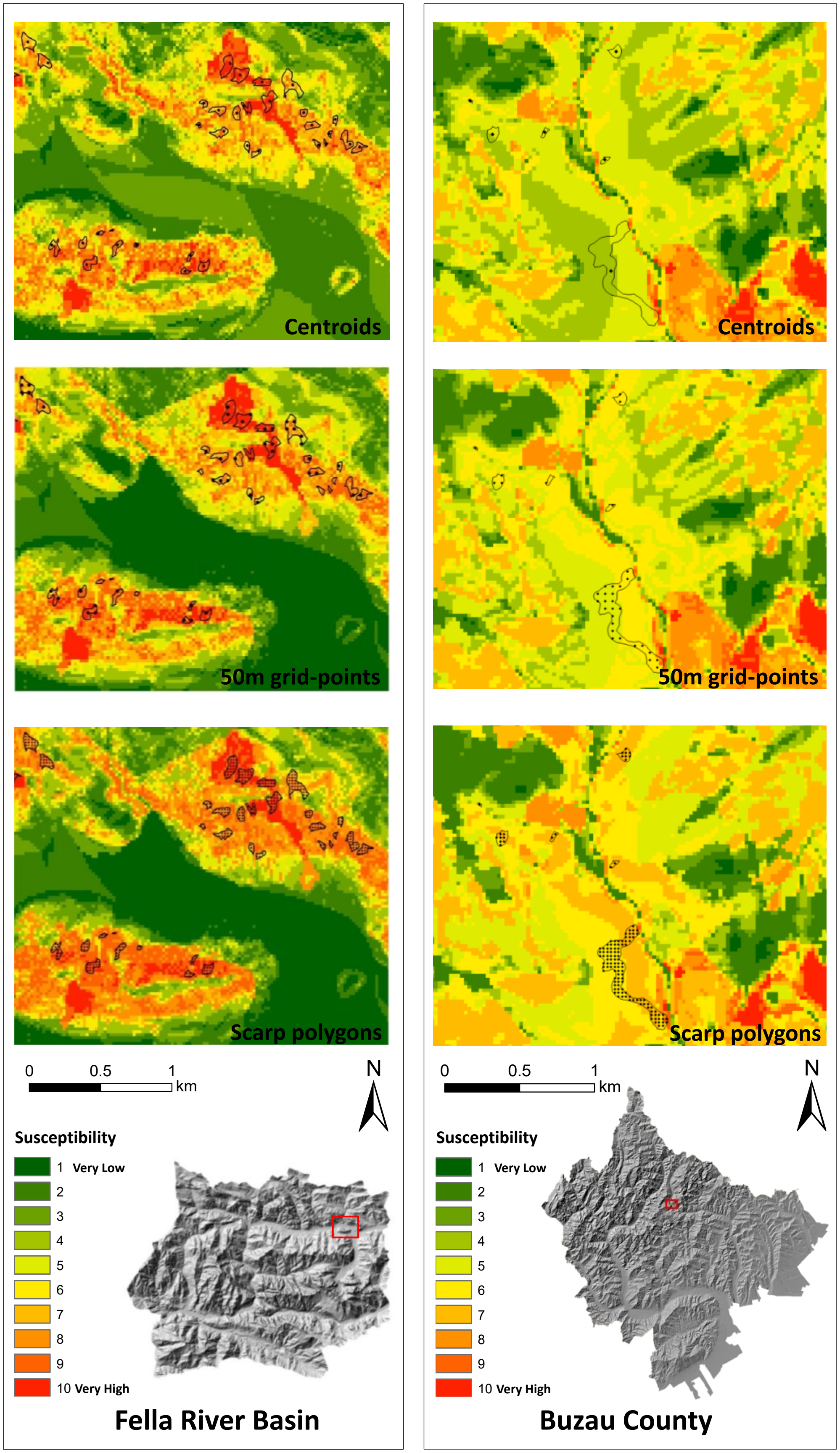
Centroids
50m grid-points
Scarp polygons
0 0.5 1 km
N
Susceptibility
1 Very Low
2
3
4
5
6
7
8
9
10 Very High
Fella River Basin
Centroids
50m grid-points
Scarp polygons
0 0.5 1 km
N
Susceptibility
1 Very Low
2
3
4
5
6
7
8
9
10 Very High
Buzau County

Figure 10 Sections of the susceptibility maps modeled using the three different types of landslide sampling strategies. From top to bottom: susceptibility modeled with scarp centroids, 50m grid-points and the landslide polygons.

The WofE model success and prediction rate curves using different landslide sampling strategies are presented in Fig 11, which also include the AUC values in percentages. For the Fella River Basin, the area under the curve (AUC) values for SRCs and PRCs show a slight increasing trend in success and prediction as the number of pixels representing the landslide scarp increases. The centroid method gives an AUC SRC of 82.53%, while modeling with the 50m grid-points and the scarp polygons give AUC values of 83.81% and 84.64% respectively. The increase in success rate is less evident in the Buzau County, with the highest AUC SRC value given by the 50m grid-points. This indicates that using the Buzau County scarp polygons should be avoided due to possible redundant information from oversampling of too many points, causing fitting problems. This coincides with a similar finding in a previous study conducted by Poli and Sterlacchini (2007). However, the prediction rate in the Buzau is highest when modeling with the entire polygon, with an AUC PRC value of 80.66%. There is little difference between the AUC SRCs and AUC PRCs, with overall the prediction rates being only slightly higher.

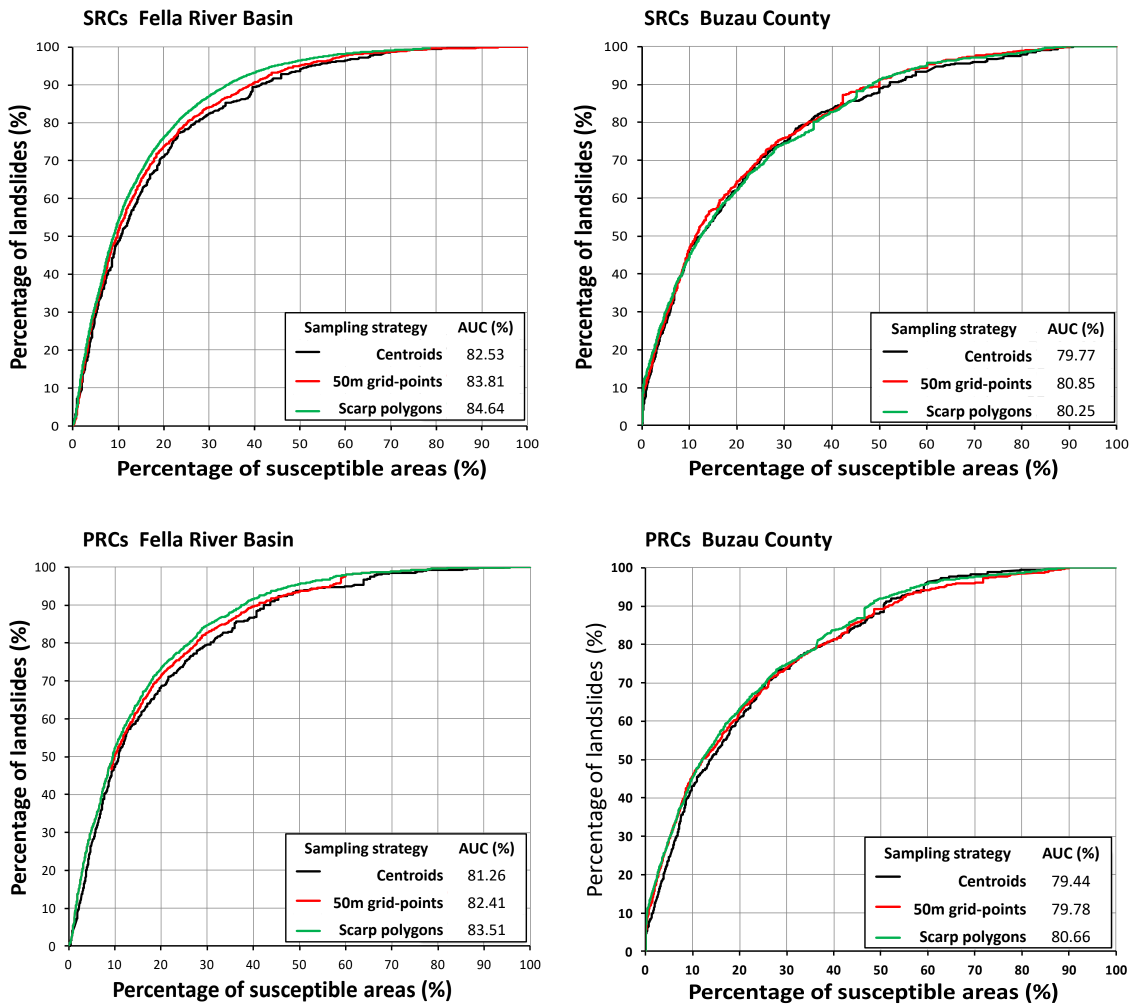


Figure 11 Success (SRC) and prediction (PRC) rate curves of the WofE susceptibility models using the three different landslide representation strategies.

Figure 12 shows a section of the susceptibility maps produced with the sample size testing. By using 52 (5%) landslides to train the model in the Fella River Basin, some areas are highly underestimated, with generalizations occurring at low to medium classes. Susceptibility maps made with 52 (5%) to 104 (10%) landslides also show grainy pixelated maps with boundaries between susceptibility classes being less continuous. It seems that when the landslide pixel sample is too small, the likelihood of random sampling from a factor class that contains more landslide pixels increases, causing a bias in the sample and possible conditional dependence problems. The abrupt shifts in the susceptibility classes which most likely follow the lithology also corresponds to the very high contrast found in the dolomite and limestone areas when using 5% of the centroid pixel inventory (Fig 6). Models using 50 to 90% perform spatially better, predicting more landslide areas and having smoother transitions from lower to higher susceptibility classes. The Buzau County susceptibility maps also show variation in medium to high susceptibility classes when increasing the number of landslides used in the WofE modeling.

Some of the low to medium susceptibility classes produced with 5 to 20% of the landslides in the Buzau County change to higher classes when using 90% of the centroid pixels.

481

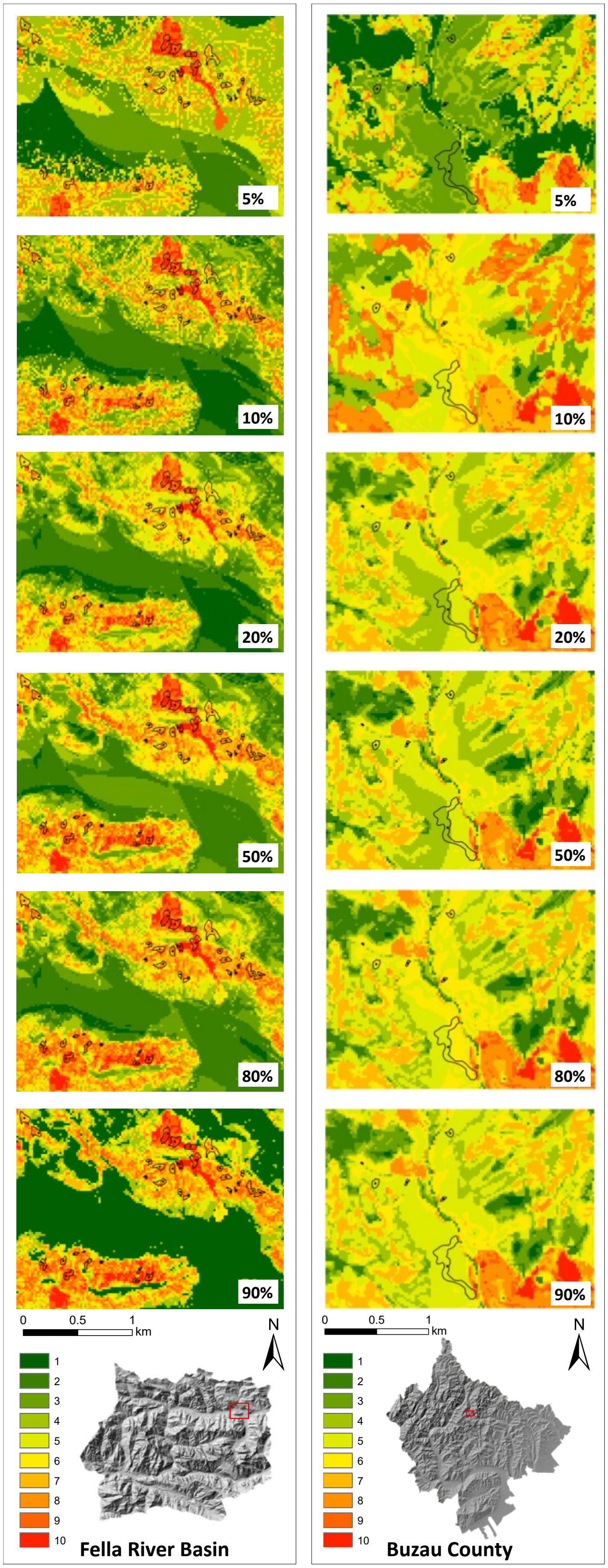
5%
10%
20%
50%
80%
90%
0
0.5
1
km
N
1
2
3
4
5
6
7
8
9
10
Fella River Basin
Buzau County

Figure 12 Sections of the landslide susceptibility maps in both study areas modeled with different sample sizes. From top to bottom: sample size percentages used were 5, 10, 20, 50, 80 and 90%. Black polygons indicate the original scarp area, with the black points indicating the centroids.

The SRCs and PRCs related to the landslide sample size sensitivity analysis are shown in Fig 13 for both study areas. The curves for the Fella River Basin indicate that as the number of landslides used to train the WofE model increases, the performance and prediction rates also increase. The trend in success and prediction rates continues to increase up to 83.87% and 82.79% respectively when using a maximum of 941 landslides for model training to predict the remaining 104 landslides. However, the strongest increase occurs when at least 104 (while 941 are used as a prediction subset) landslides are used to train the model, producing an AUC SRC value of 81.45% and an AUC PRC value of 81.73%. This indicates that when using the WofE model in the Fella River Basin, 104 landslides are enough to accurately predict the occurrence of the rest of the 941 landslides used as a prediction subset. In the Buzau County, the best success rates are obtained using at least 322 landslides to train the model, while the best prediction is made using a 50/50 % ratio between the number of training and prediction landslides. The Buzau County does not indicate a clear increasing trend in success and prediction when compared to the Fella River.

The random sampling of the landslide centroids used to train the WofE model was carried out only once for each sample size. To study the effect of the sampling procedure, we took 10 random samples for each sample size in the Fella River Basin. The results of the success and prediction rates for the 10 random samples of all sample sizes is shown in Table 3. The mean AUC values show an increase as the number of landslides are increased to train the model. There is also a significant decrease in the standard deviation of the 10 random samples when using 200 or more landslides. The AUC prediction rates show a similar increase as the success rates. The overall trend in AUC values with 10 random samples is still similar to using a single random sample for each landslide sample size.

Fig. 14 graphically shows the AUC values related to the success and prediction rate curves in Fig. 13 for the Buzau County and the average values in Table 3 for the Fella River Basin. As the number of landslides used to train the model in the Fella River increases up to 100, the AUC value rapidly increases from 61 to 82%. After using 100 to 200 landslides, the increase in AUC is very gradual with a “plateau effect” visible in the performance and prediction rates. This effect is not visible in the AUC success rates Buzau County, with only a 5% increase in AUC prediction rate from 75 to 80% when increasing the training sample from 100 to 800 landslides. However, in the Buzau County after training the model with more 1400 landslides, a drop in the prediction rate occurs from 79 to 76%, when trying to validate the remaining 160 landslides.

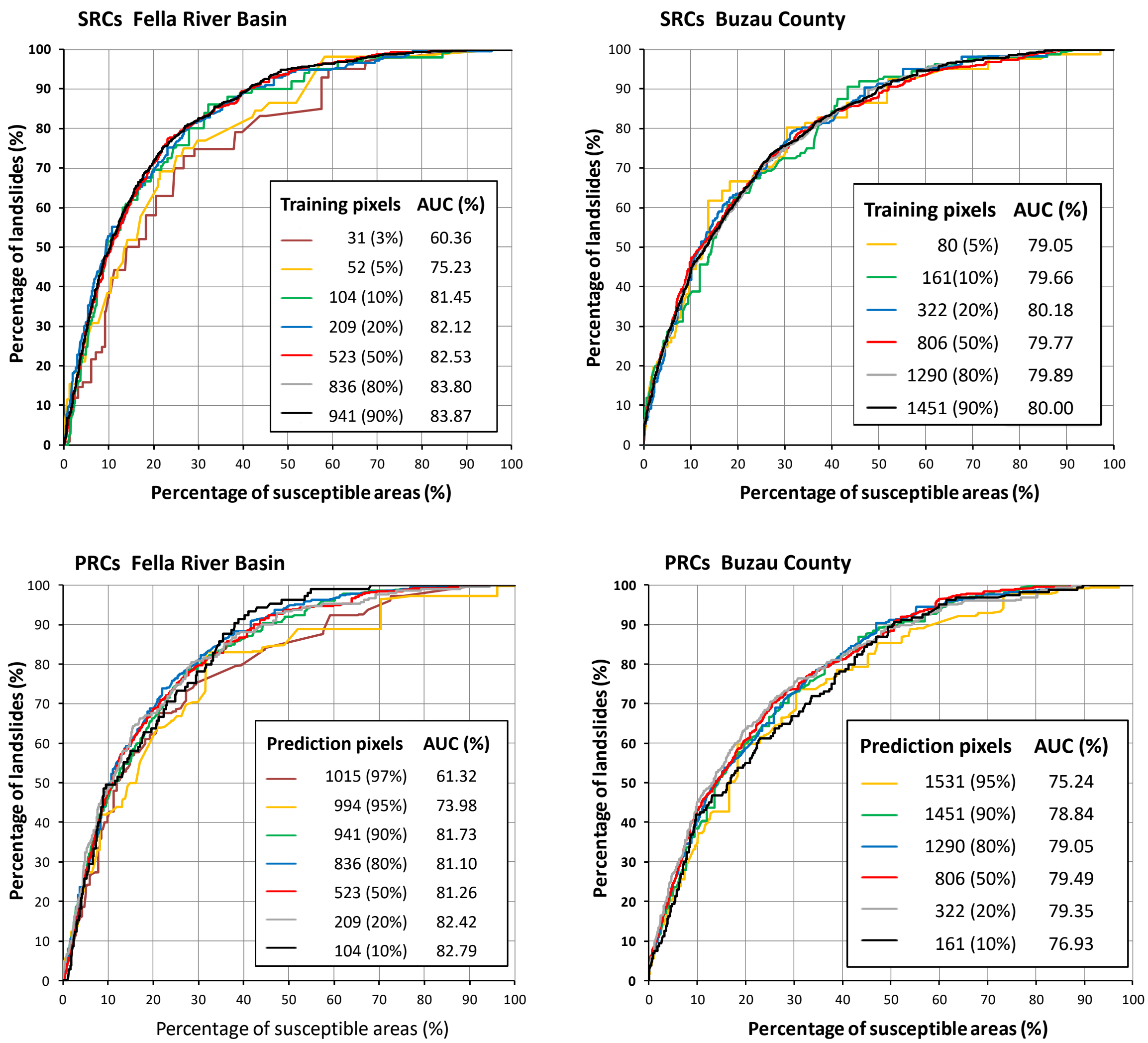


Figure 13 SRCs, PRCs and AUC values for susceptibility maps modeled with different landslide sample sizes.

Table 3 Weights-of-Evidence susceptibility success and prediction rates for ten random samples of each landslide sampling size in the Fella River Basin study area. The table has information on the statistics of the success and prediction rates, including the mean value of the 10 models for each sampling size and the standard deviation .

| **Number of landslides used for model training** | **% of all landslides** | **Area under the success rate curve (%), SRC AUC** | | | | | | | | | | **Statistics for the 10 model runs** | |
|---|---|---|---|---|---|---|---|---|---|---|---|---|---|
| | | **1** | **2** | **3** | **4** | **5** | **6** | **7** | **8** | **9** | **10** | **Mean** | **Std** |
| 31 | 3 | 60,36 | 59,45 | 61,81 | 59,33 | 59,06 | 59,80 | 59,84 | 61,42 | 59,08 | 60,66 | 60,08 | 0,96 |
| 52 | 5 | 75,23 | 75,49 | 75,89 | 72,28 | 75,33 | 74,68 | 74,37 | 73,06 | 76,61 | 73,45 | 74,64 | 1,36 |
| 104 | 10 | 81,45 | 79,91 | 79,18 | 77,76 | 82,25 | 80,63 | 78,27 | 80,45 | 80,92 | 78,95 | 79,98 | 1,43 |
| 209 | 20 | 82,12 | 81,90 | 82,01 | 82,57 | 82,32 | 81,75 | 82,37 | 81,81 | 82,68 | 82,91 | 82,24 | 0,39 |
| 523 | 50 | 82,53 | 83,19 | 82,03 | 82,48 | 82,95 | 82,38 | 82,21 | 83,00 | 82,08 | 83,10 | 82,60 | 0,44 |
| 836 | 80 | 83,80 | 83,20 | 83,34 | 83,86 | 83,82 | 83,69 | 82,90 | 82,58 | 83,94 | 83,32 | 83,45 | 0,46 |
| 941 | 90 | 83,87 | 84,79 | 83,53 | 83,93 | 84,15 | 83,04 | 84,64 | 83,03 | 84,40 | 84,65 | 84,00 | 0,65 |
| | | | | | | | | | | | | | |
| **Number of landslides used for model prediction** | **% of all landslides** | **Area under the prediction rate curve (%), PRC AUC** | | | | | | | | | | **Statistics for the 10 model runs** | |
| | | **1** | **2** | **3** | **4** | **5** | **6** | **7** | **8** | **9** | **10** | **Mean** | **Std** |
| 1015 | 97 | 61,32 | 59,10 | 59,87 | 62,27 | 60,82 | 59,33 | 60,45 | 60,45 | 60,32 | 59,13 | 60,31 | 1,01 |
| 994 | 95 | 73,98 | 71,18 | 73,99 | 70,66 | 74,99 | 75,98 | 70,73 | 75,87 | 70,29 | 74,64 | 73,23 | 2,27 |
| 941 | 90 | 81,73 | 82,00 | 81,17 | 81,77 | 81,10 | 80,71 | 81,94 | 80,53 | 80,12 | 80,69 | 81,18 | 0,66 |
| 836 | 80 | 81,10 | 81,15 | 81,07 | 81,11 | 81,43 | 81,57 | 80,69 | 81,79 | 81,48 | 80,41 | 81,18 | 0,41 |
| 523 | 50 | 81,26 | 80,83 | 81,88 | 81,84 | 80,98 | 81,45 | 80,90 | 81,94 | 81,20 | 81,81 | 81,41 | 0,43 |
| 209 | 20 | 82,42 | 82,64 | 81,96 | 81,57 | 82,37 | 82,82 | 82,26 | 82,01 | 82,40 | 82,41 | 82,29 | 0,36 |
| 104 | 10 | 82,79 | 83,81 | 83,43 | 83,91 | 83,36 | 83,73 | 83,18 | 83,73 | 82,87 | 82,92 | 83,37 | 0,42 |

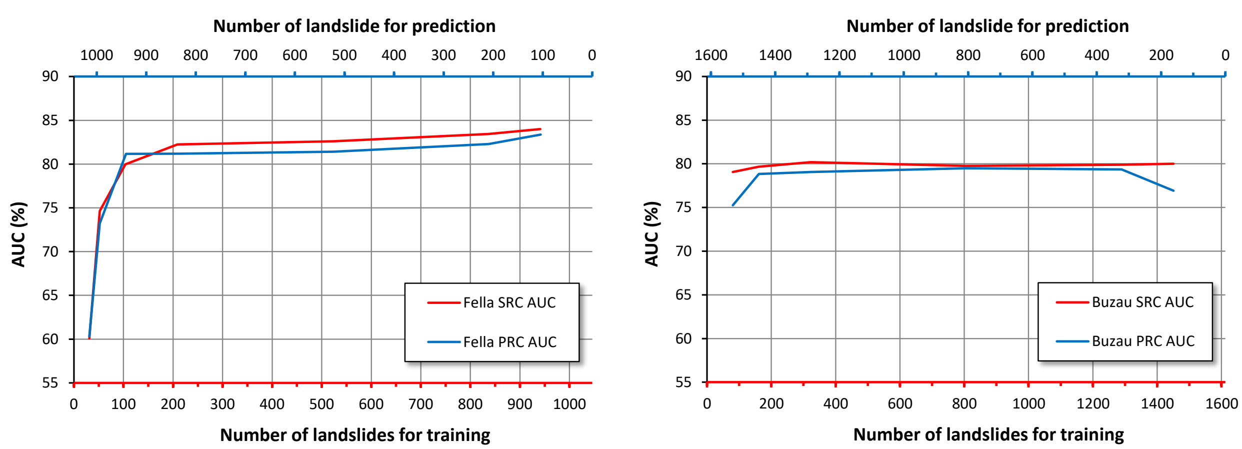


Figure 14 The AUC values of the success rate (SRCs) and prediction rate (PRCs) curves for susceptibility models trained with different number of landslides from the available inventories. The red curves indicate the model success rates for different landslide training sizes and the blue curves indicate the model prediction rates using different landslide prediction sample sizes.

# 7. Discussion

The weights assigned to each class within a causative factor map in the WofE model is determined by the number of landslide pixels counted in each class and the difference in the number of pixels between the classes. The tests carried out using different sampling strategies basically increases the number of pixels that are assigned to each landslide for susceptibility modeling, thereby increasing the landslide area in a causative factor class. The results in Fig 11 show in the Fella River Basin that there is a slight increase in success and prediction rates associated with the increase in pixels representing the landslide scarp polygons. This is in agreement with findings in previous studies (Poli and Sterlacchini, 2007; Thiery et al., 2007; Yilmaz, 2010; Regmi et al., 2013). However, this increase is not evident in the Buzau County, where there is no change in model performance between the use of centroids and scarp polygons (Fig 11). Despite a significant increase in the number of landslide pixels to represent the entire landslide scarp polygon, there is overall little difference in model performance and prediction between the sampling strategies.

In order to understand these results, Table 4 is required, which shows the percentage increase in number of landslide pixels as the sampling strategy changes for two causative factors in both case study areas. These are land cover and lithology for the Fella River Basin, and land cover and soil for the Buzau County. The percentage increase for most factor classes is very similar, particularly in the classes that have many pixels. This similarity will cause very little change in the weights of the individual factor map classes when increasing the pixels for different sampling strategies. This is most likely due to the scarp polygons having similar sizes through-out the study area. If the landslide scarp polygons are of similar size throughout the study area, the relative increase in the number of pixels to represent each polygon will be similar for all the scarps. Changing the representation of a single scarp in a certain factor class from one pixel to, for example, 10 pixels, will allocate a similar increase in pixels to a scarp polygon located in a different class. The chances of this problem occurring can be high because landslide susceptibility assessments are mainly carried out using a single landslide type, without mixing landslides of different types and therefore different sizes.

Table 4 also gives us an indication why our model performs slightly better in the Fella River Basin when we change the sampling strategy, compared to the Buzau County. The average percentage increase in the number of pixels in each factor class from the centroid strategy to 50m grid points in the Fella River Basin is 414%, while the average increase from 50m grid-points to the polygon strategy (all pixels) is 527%. However, in the Buzau County, the percentage increases for the same tests are 102% and 190% respectively. In other words, the landslide area in the Buzau County increases 2 to 3 times more when using polygons instead of centroids, while in the Fella River Basin, the area increases 5 to 6 times. This much larger increase in landslide size in the pixel representation, despite being relatively similar through-out the study area, will still show some significance in success and prediction rates of the susceptibility model compared to that of the Buzau County. Thus, the size of the area, the scale of the study and the quality of the data can have significant effects on the landslide susceptibility mapping accuracy (Catani et al., 2013; Petschko et al., 2013).

Table 4 Number of landslide pixels located within the geo-environmental factor map classes. The factors are land cover and lithology for the Fella River Basin and land cover and soil for the Buzau County. The last two columns on the right indicate the percentage increase in the number of pixels when changing the strategy from centroid to 50m grid-points and from 50m grid-points to using the entire scarp polygon (considering all pixels within the polygon) respectively.

| **Fella River Basin** | | | | | |
|---|---|---|---|---|---|
| **Land cover** | **Centroid pixels** | **50m grid-point pixels** | **All scarp pixels** | **Percent increase centroid --> 50m** | **Percent increase 50m --> all pixels** |
| Human infrastructure | 0 | 0 | 0 | - | - |
| Agriculture | 0 | 0 | 0 | - | - |
| Flood plain | 2 | 3 | 17 | 50% | 467% |
| Woodland | 44 | 148 | 922 | 236% | 523% |
| Grassland | 70 | 365 | 2279 | 421% | 524% |
| Forest | 157 | 729 | 4535 | 364% | 522% |
| Bare rock | 250 | 1485 | 9199 | 494% | 519% |
| **Lithology** | **Centroid pixels** | **50m grid-point pixels** | **All scarp pixels** | **Percent increase centroid --> 50m** | **Percent increase 50m --> all pixels** |
| Alluvial deposits | 0 | 10 | 53 | - | 430% |
| Intrusive rocks | 0 | 6 | 30 | - | 400% |
| Mud- and sandstones | 1 | 10 | 56 | 900% | 560% |
| Conglomerates | 4 | 9 | 77 | 225% | 756% |
| Marls | 11 | 49 | 318 | 345% | 549% |
| Debris and scree deposits | 23 | 147 | 933 | 539% | 534% |
| Dolomitic marls | 45 | 327 | 2149 | 627% | 557% |
| Dolomite and dolomitic limestones | 439 | 2172 | 13336 | 395% | 514% |
| | | | | | |
| **Buzau County** | | | | | |
| **Land cover** | **Centroid pixels** | **50m grid-point pixels** | **All scarp pixels** | **Percent increase centroid --> 50m** | **Percent increase 50m --> all pixels** |
| vineyards | 0 | 0 | 1 | - | - |
| bushes | 1 | 7 | 35 | 600% | 400% |
| roads | 7 | 7 | 21 | 0% | 200% |
| orchards | 12 | 13 | 36 | 8% | 176% |
| houses-households | 18 | 26 | 40 | 44% | 54% |
| wetlands-waters | 24 | 32 | 75 | 33% | 134% |
| degraded land-bare rock | 36 | 104 | 331 | 189% | 218% |
| forest | 206 | 330 | 1011 | 60% | 206% |
| pastures-hayfields | 497 | 713 | 1988 | 43% | 179% |
| **Soil** | **Centroid pixels** | **50m grid-point pixels** | **All scarp pixels** | **Percent increase centroid --> 50m** | **Percent increase 50m --> all pixels** |
| AP | 0 | 0 | 0 | - | - |
| SN/BR/RP | 3 | 3 | 7 | 0% | 133% |
| PD/SP | 4 | 4 | 13 | 0% | 225% |
| BD/CI | 6 | 6 | 16 | 0% | 167% |
| SC | 7 | 10 | 30 | 43% | 200% |
| SA/AA | 23 | 41 | 85 | 78% | 107% |
| CN/NF/LC | 41 | 68 | 240 | 66% | 253% |
| BP/PB | 80 | 142 | 408 | 78% | 187% |
| BO/CC/CZ/NO | 112 | 187 | 628 | 67% | 236% |
| BM/RS/LS/PS | 246 | 361 | 1013 | 47% | 181% |
| PR/ER/RZ | 279 | 413 | 1106 | 48% | 168% |

The sampling strategy tests show similarities between the area under the SRCs and PRCs curves (AUC). When the WofE model has similar performance values as the prediction values, this indicates that both training and prediction subsets fit the model equally well. This is most likely due to the pixels being sampled from the same landslide polygon causing for both subsets to perform similarly. Training and prediction pixels represent more or less the same causative factor combinations which will produce similar success and prediction rates curves of the susceptibility model. This indicates that it is recommended to randomly sample entire polygons into separate success and prediction subsets so that pixels from a single polygon are not separated from each other and thereby decreasing the possibility of oversampling or over fitting. This problem has been most recently described by San (2014) where he indicates that "polygon-based random sampling is recommended for collecting the training and testing data", and therefore is preferred over pixel based random sampling as has been used in this paper. However, we have avoided this problem when using only the centroids in the sample size sensitivity tests.

The sampling strategy tests using different sample sizes to train the WofE model show that there are a minimum number of landslides needed to produce sufficient model performance and prediction results. Figure 14 indicates that in the Fella River Basin, there is a minimum of 104 to 209 (10 to 20% of the inventory) out of a total of 1046 landslide centroids required to produce success and prediction rate curves with AUC values above 80%. Using more than 104 centroid pixels slightly increases the AUC for performance and prediction but starts to show a plateau with little changes in the overall values after using 200 or more landslide centroids. This plateau in performance corresponds well with recent previous studies (Hjort and Marmion, 2008; Guns and Vanacker, 2012; Heckmann et al., 2014; Petschko et al., 2014).

The Buzau county AUC SRCs do not show a clear trend as in the Fella River, with a peak AUC SRC of 80.18% found when using 322 from a total of 1612 landslide centroids (Fig. 14). However, the AUC PRCs in the Buzau County do indicate that a minimum of 161 landslides are needed for an acceptable prediction rate of 78.84%, while more training landslides produce a similar plateau as seen in the Fella River. The Buzau County susceptibility map trained with 80 landslides has difficulties predicting the remaining 1531 landslides. As expected, the AUC values of the SRCs in both areas are generally slightly higher than the AUC values of the PRCs. It is interesting to note that in the Buzau County, when training the model with 1531 landslides to predict the remaining 80, the prediction rate decreased from 79.35 to 76.93%. A possible reason for this drop could be that the much larger Buzau County has an uneven distribution of mapped landslides, where the Northern part of the County is less represented in the mapping process. Furthermore, there are also possible mapping inaccuracies and incompleteness in the landslide inventory. The Buzau County success and prediction rates could be improved if many random samples would have been conducted as in the Fella River. It is therefore recommended to carry out many random samples for both areas in the future, possibly up to 50, 100 or even 1000 model runs (Brenning, 2005; Beguería, 2006; Van Den Eeckhaut et al., 2010; Heckmann et al., 2014), to get a more accurate view on the effects of sampling different landslide sample sizes on the success and prediction rate of the susceptibility model.

By conducting the sample size tests, we have analyzed the performance of the WofE model to changes in the ratio between landslide training and prediction pixels. The analysis has shown that for two areas with completely different sizes (~765 $km^2$ and ~3231 $km^2$) and landslide types (debris flows vs. shallow landslides), a training to prediction subset ratio of 1:9 (10% : 90%) produces sufficient model performance and prediction, with both areas containing more than 1000 landslide centroid grid-points (pixels). The use of 10% of the landslide inventory equals to 161 landslide pixels in the Buzau County and 104 pixels in the Fella River Basin. This corresponds with a landslide to non-landslide pixel ratio of 1:32105 and 1:18208, respectively.

Overall, the WofE landslide susceptibility model has performed slightly better with the debris flows in the Fella River Basin than with the shallow landslides of the Buzau County. As the landslide pixel sampling strategy increased from a single centroid to the entire polygon, so did the success and prediction of the debris flow source areas slightly increase, with most debris flow sources also significantly increasing in the number of pixels. In the Buzau County, the shallow landslides did not show this significant increase in pixels representing the scarp areas. This indicates that the scarp areas of the shallow landslides are too small for the given mapping unit of 25m. Thus, the scale and resolution of the mapping unit are a very important issue in landslide susceptibility mapping and prediction (Catani et al., 2013). An advisable mapping resolution would have been 10m  or even 5m to better capture the effects of the sampling strategies on the model success and prediction.

The maximum obtained success and prediction rates using different landslide centroid sample sizes were higher for the Fella River Basin than the Buzau County. The increase in the model performance when increasing the number of landslides used for model training were much more significant for the debris flows than the shallow landslides. However, in the future, more susceptibility models should be run in the Buzau County for smaller sample sizes  (< 100 landslides) too better study the significance of possible sample size thresholds in larger areas which have been known to occur in previous studies (Hjort and Marmion, 2008; Heckmann et al., 2014).

Even with similarities in modeled success and prediction rates found in the landslide sampling strategies, there are still some visible differences in the classified susceptibility maps. This indicates that the spatial variation between the similar performing susceptibility maps can be different. A susceptibility map trained with 100 landslides can give similar performance rates (AUC values) as a map made using 500 landslides but still looks very different after classifying the maps using the same method. A spatial agreement analysis (Sterlacchini et al., 2011) can be carried out in future studies in order to determine the best susceptibility classification by taking into consideration all maps that show similar performance and prediction rates. This is important in order to communicate to decision-makers, land-use planners and responsible authorities the right maps to assess landslide hazard and risk.

## 7. Conclusions

The Weights-of-Evidence landslide susceptibility model has shown to be flexible in its application in areas that are very different in terms of size, geo-environmental settings and landslide types. The model was applied in the Italian Alps using debris flow scarps and in the Romanian Carpathians using shallow landslides. Three different landslide sampling strategies were tested in the susceptibility analysis: (1) the centroid scarp point, (2) points located every 50 m within the scarp and using (3) the entire scarp polygon. The shallow landslides in the Buzau County (Romanian Carpathians) gave better success rates when sampled using the 50m grid-point method, while the scarp polygon method was better in predicting the shallow landslides. The susceptibility model assessing the debris flow scarps in the Fella River Basin (Italian Alps) had better success and prediction rates when using the entire scarp polygon, compared to the other strategies. Overall, the model performed better using debris flows scarps than the shallow landslides. The number of landslides were similar for both case studies, however, the Romanian site was 4 times larger with some areas being underrepresented in terms of mapping and quality of the data.

A sensitivity analysis was also conducted in both study areas to test the effect of the landslide sample size used to train the model on the susceptibility performance rates. In the Fella River Basin, a training subset threshold of 104 debris flow scarps were sufficient to predict the remaining 941 scarps, giving success and prediction rates (AUC values) above 81%. The Buzau county required a training subset of at least 161 shallow landslide scarps to predict the remaining 1451 scarps with success and prediction rates above 79%. When training subsets were used that contained landslide numbers below these thresholds, model performance was significantly lower. However, using more landslides above the thresholds caused success and prediction rates to "plateau" with only slight increase in model performance.

The comparison of the classified susceptibility maps produced using different sampling strategies and sample sizes indicated that there are significant differences in the lower to medium susceptibility classes despite having similar success and prediction rate values. It is therefore recommended in the future to combine the maps in order assess where they spatially agree and how they can be used for decision-makers.

## Acknowledgements

This study is part of an ongoing landslide quantitative risk assessment (QRA) carried out within the EC FP-7 funded CHANGES network (Grant Agreement No. 263953).

# References

Akgun, A., 2012. A comparison of landslide susceptibility maps produced by logistic regression, multi-criteria decision, and likelihood ratio methods: a case study at İzmir, Turkey. Landslides, 9(1), 93-106.

Aleotti, P., Chowdhury, R., 1999. Landslide hazard assessment: summary review and new perspectives. Bull Eng Geol Environ, 58(1), 21-44.

ANCPI, 2014. National Agency for Cadastre and Land Registration.

Atkinson, P.M., Massari, R., 1998. GENERALISED LINEAR MODELLING OF SUSCEPTIBILITY TO LANDSLIDING IN THE CENTRAL APENNINES, ITALY. Computers & Geosciences, 24(4), 373-385.

Ayalew, L., Yamagishi, H., 2005. The application of GIS-based logistic regression for landslide susceptibility mapping in the Kakuda-Yahiko Mountains, Central Japan. Geomorphology, 65(1–2), 15-31.

Beguería, S., 2006. Validation and Evaluation of Predictive Models in Hazard Assessment and Risk Management. Natural Hazards, 37(3), 315-329.

Blahut, J., van Westen, C.J., Sterlacchini, S., 2010. Analysis of landslide inventories for accurate prediction of debris-flow source areas. Geomorphology, 119(1–2), 36-51.

Bonham-Carter, G.F., Agterberg, F.P., Wright, D.F., 1988. Integration of geological datasets for gold exploration in Nova Scotia. Photogrammetric Engineering and Remote Sensing, 54(11), 1585-1592.

Bonham-Carter, G.F., Agterberg, F.P., Wright, D.F., 1989. Weights of evidence modelling: a new approach to mapping mineral potential. In: D.F. Agterberg, G.F. Bonham-Carter (Eds.), Statistical Applications in Earth Sciences. Geological Survey of Canada, Ottowa.

Borga, M., Boscolo, P., Zanon, F., Sangati, M., 2007. Hydrometeorological analysis of the August 29, 2003 flash flood in the eastern Italian Alps. Journal of Hydrometeorology, 8, 1049 - 1067.

Borga, M., Gaume, E., Creutin, J.D., Marchi, L., 2008. Surveying flash floods: gauging the ungauged extremes. Hydrological Processes, 22, 3883 - 3885.

Brenning, A., 2005. Spatial prediction models for landslide hazards: review, comparison and evaluation. Nat. Hazards Earth Syst. Sci., 5(6), 853-862.

Brenning, A., 2009. Benchmarking classifiers to optimally integrate terrain analysis and multispectral remote sensing in automatic rock glacier detection. Remote Sensing of Environment, 113(1), 239-247.

Calligaris, C., Boniello, M.A., Zini, L., 2008. Debris flow modelling in Julian Alps using FLO-2D. In: D. De Wrachien, C.A. Brebbia, M.A. Lenzi (Eds.), Monitoring, simulation, prevention and remediation of dense and debris flows II. Witpress, Southhampton, UK, pp. 81-88.

Capitani, M., Federici, P., 2013. MSUE Conditional Method Predictive Power, Milia Basin, Tuscany, Italy. In: C. Margottini, P. Canuti, K. Sassa (Eds.), Landslide Science and Practice. Springer Berlin Heidelberg, pp. 511-517.

Capitani, M., Ribolini, A., Federici, P.R., 2013. Influence of deep-seated gravitational slope deformations on landslide distributions: A statistical approach. Geomorphology, 201(0), 127-134.

Carrara, A., 1983. Multivariate models for landslide hazard evaluation. Journal of the International Association for Mathematical Geology, 15(3), 403-426.

Carrara, A., Cardinali, M., Guzzetti, F., Reichenbach, P., 1995. Gis Technology in Mapping Landslide Hazard. In: A. Carrara, F. Guzzetti (Eds.), Geographical Information Systems in Assessing Natural Hazards. Advances in Natural and Technological Hazards Research. Springer Netherlands, pp. 135-175.

Carrara, A., Crosta, G., Frattini, P., 2008. Comparing models of debris-flow susceptibility in the alpine environment. Geomorphology, 94(3–4), 353-378.

Castellanos Abella, E.A., de Jong, S.M., van Westen, C.J., van Asch, T.W.J., 2008. Multi - scale landslide risk assessment in Cuba. ITC PhD Dissertation 154, . ITC Enschede, University of Utrecht, Utrecht.

Catani, F., Lagomarsino, D., Segoni, S., Tofani, V., 2013. Landslide susceptibility estimation by random forests technique: sensitivity and scaling issues. Nat. Hazards Earth Syst. Sci., 13(11), 2815-2831.

Chalkias, C., Ferentinou, M., Polykretis, C., 2014. GIS Supported Landslide Susceptibility Modeling at Regional Scale: An Expert-Based Fuzzy Weighting Method. ISPRS International Journal of Geo-Information, 3(2), 523-539.

Chung, C.-J., Fabbri, A.G., 1999. Probabilistic prediction models for landslide hazard mapping. In: A. Buccianti, G. Nardi, R. Potenza (Eds.), Proceedings of International Association for Mathematical Geology 1998 Annual Meeting (IAMG'98), Ischia, Italy, October 1998,, pp. 203-211.

Chung, C.-J., Fabbri, A.G., 2003. Validation of Spatial Prediction Models for Landslide Hazard Mapping. Natural Hazards, 30(3), 451-472.

Chung, C.-J., Fabbri, A.G., 2005. Systematic Procedures of Landslide Hazard Mapping for Risk Assessment Using Spatial Prediction Models, Landslide Hazard and Risk. John Wiley & Sons, Ltd, pp. 139-174.

Clerici, A., 2002. A GRASS GIS based shell script for landslide susceptibility zonation. In: M. Ciolli, P. Zatelli (Eds.), Proceedings of the open source free software GIS-GRASS users conference, Trento, Italy 11-13 September 2002, Trento, Italy.

Clerici, A., Perego, S., Tellini, C., Vescovi, P., 2006. A GIS-based automated procedure for landslide susceptibility mapping by the Conditional Analysis method: the Baganza valley case study (Italian Northern Apennines). Environmental Geology, 50(7), 941-961.

Clerici, A., Perego, S., Tellini, C., Vescovi, P., 2010. Landslide failure and runout susceptibility in the upper T. Ceno valley (Northern Apennines, Italy). Natural Hazards, 52(1), 1-29.

CNR-IRPI, 2014. AVI Project.

Corominas, J., Westen, C., Frattini, P., Cascini, L., Malet, J.P., Fotopoulou, S., Catani, F., Eeckhaut, M., Mavrouli, O., Agliardi, F., Pitilakis, K., Winter, M.G., Pastor, M., Ferlisi, S., Tofani, V., Hervás, J., Smith, J.T., 2013. Recommendations for the quantitative analysis of landslide risk. Bull Eng Geol Environ, 1-55.

Creutin, J.D., Borga, M., 2003. Radar hydrology modifies the monitoring of flash flood hazard. Hydrological Processes, 17, 1453 - 1456.

Crozier, M.J., Glade, T., 2005. Landslide Hazard and Risk: Issues, Concepts and Approach, Landslide Hazard and Risk. John Wiley & Sons, Ltd, pp. 1-40.

Dai, F.C., Lee, C.F., Ngai, Y.Y., 2002. Landslide risk assessment and management: an overview. Engineering Geology, 64(1), 65-87.

Demir, G., Aytekin, M., Akgün, A., İkizler, S., Tatar, O., 2013. A comparison of landslide susceptibility mapping of the eastern part of the North Anatolian Fault Zone (Turkey) by likelihood-frequency ratio and analytic hierarchy process methods. Natural Hazards, 65(3), 1481-1506.

Donati, L., Turrini, M.C., 2002. An objective method to rank the importance of the factors predisposing to landslides with the GIS methodology: application to an area of the Apennines (Valnerina; Perugia, Italy). Engineering Geology, 63(3–4), 277-289.

EEA, 2014. CORINE Land Cover programme of the European Environment Agency.

Felicísimo, Á., Cuartero, A., Remondo, J., Quirós, E., 2013. Mapping landslide susceptibility with logistic regression, multiple adaptive regression splines, classification and regression trees, and maximum entropy methods: a comparative study. Landslides, 10(2), 175-189.

Fell, R., Corominas, J., Bonnard, C., Cascini, L., Leroi, E., Savage, W.Z., 2008. Guidelines for landslide susceptibility, hazard and risk zoning for land-use planning. Engineering Geology, 102(3–4), 99-111.

Florea, N., Munteanu, I., 2000. Sistemu Roman de Taxonomie a Solurilor (Romanian System of Soil Taxonomy), Univ. "Al. I. Cuza" Iasi. 107.

Galli, M., Ardizzone, F., Cardinali, M., Guzzetti, F., Reichenbach, P., 2008. Comparing landslide inventory maps. Geomorphology, 94(3–4), 268-289.

Galve, J., Cevasco, A., Brandolini, P., Soldati, M., 2014. Assessment of shallow landslide risk mitigation measures based on land use planning through probabilistic modelling. Landslides, 1-14.

Georgescu, E.S., 2002. Towards an earthquake insurance system in Romania. In: D. Lungu, F. Wenzel (Eds.), Earthquake loss estimation and risk reduction, Proceedings of the international conference on Vrancea Earthquakes, Bucharest, Romania.

Glade, T., Crozier, M.J., 2005. A Review of Scale Dependency in Landslide Hazard and Risk Analysis, Landslide Hazard and Risk. John Wiley & Sons, Ltd, pp. 75-138.

Gorum, T., Fan, X., van Westen, C.J., Huang, R.Q., Xu, Q., Tang, C., Wang, G., 2011. Distribution pattern of earthquake-induced landslides triggered by the 12 May 2008 Wenchuan earthquake. Geomorphology, 133(3–4), 152-167.

Guns, M., Vanacker, V., 2012. Logistic regression applied to natural hazards: rare event logistic regression with replications. Nat. Hazards Earth Syst. Sci., 12(6), 1937-1947.

Guzzetti, F., Carrara, A., Cardinali, M., Reichenbach, P., 1999. Landslide hazard evaluation: a review of current techniques and their application in a multi-scale study, Central Italy. Geomorphology, 31(1–4), 181-216.

Guzzetti, F., Reichenbach, P., Cardinali, M., Galli, M., Ardizzone, F., 2005. Probabilistic landslide hazard assessment at the basin scale. Geomorphology, 72(1–4), 272-299.

Heckmann, T., Gegg, K., Gegg, A., Becht, M., 2014. Sample size matters: investigating the effect of sample size on a logistic regression susceptibility model for debris flows. Nat. Hazards Earth Syst. Sci., 14(2), 259-278.

Hjort, J., Marmion, M., 2008. Effects of sample size on the accuracy of geomorphological models. Geomorphology, 102(3–4), 341-350.

Hussin, H.Y., Zumpano, V., Sterlacchini, S., Reichenbach, P., Bãlteanu, D., Micu, M., Bordogna, G., Cugini, M., 2013. Comparing the predictive capability of landslide susceptibility models in three different study areas using the Weights of Evidence technique. Geophysical Research Abstracts, Vol. 15, EGU2013-12701-1.

ICPA, 2014. The Research Institute for Soil Science and Agrochemistry.

ISPRA, 2014. The IFFI project (Inventory of Landslide Phenomena in Italy).

JRC, 2014. MOLAND - Monitoring Land Use/Cover Dynamics.

Jurko, J., Paudits, P., Vlcko, J., 2006. Landslide susceptibility map of Liptovska kotlina basin using GIS. In: M. Culshaw, H. Reeves, T. Spink, I. Jefferson (Eds.), IAEG2006, Engineering geology for tomorrow's cities. The Geological Society of London, Nottingham, United Kingdom, pp. 162.

Lee, S., 2005. Application and cross-validation of spatial logistic multiple regression for landslide susceptibility analysis. Geosciences Journal, 9(1), 63-71.

Lee, S., Choi, J., 2004. Landslide susceptibility mapping using GIS and the weight-of-evidence model. International Journal of Geographical Information Science, 18(8), 789-814.

Lee, S., Choi, J., Min, K., 2002. Landslide susceptibility analysis and verification using the Bayesian probability model. Environmental Geology, 43(1-2), 120-131.

Lee, S., Choi, J., Woo, I., 2004. The effect of spatial resolution on the accuracy of landslide susceptibility mapping: a case study in Boun, Korea. Geosciences Journal, 8(1), 51-60.

Lee, S., Digna, G.E., 2005. Landslide susceptibility mapping using probability and statistics models in Baguio City. 31st International Symposium on Remote Sensing of Environment, Saint Petersburg, Russia.

Legorreta Paulin, G., Bursik, M., Lugo-Hubp, J., Zamorano Orozco, J.J., 2010. Effect of pixel size on cartographic representation of shallow and deep-seated landslide, and its collateral effects on the forecasting of landslides by SINMAP and Multiple Logistic Regression landslide models. Physics and Chemistry of the Earth, Parts A/B/C, 35(3–5), 137-148.

Malek, Ž., Scolobig, A., Schröter, D., 2014. Understanding Land Cover Changes in the Italian Alps and Romanian Carpathians Combining Remote Sensing and Stakeholder Interviews. Land, 3(1), 52-73.

Martha, T.R., van Westen, C.J., Kerle, N., Jetten, V., Vinod Kumar, K., 2013. Landslide hazard and risk assessment using semi-automatically created landslide inventories. Geomorphology, 184(0), 139-150.

Melchiorre, C., Matteucci, M., Azzoni, A., Zanchi, A., 2008. Artificial neural networks and cluster analysis in landslide susceptibility zonation. Geomorphology, 94(3–4), 379-400.

Micu, M., Bălteanu, D., 2013. A deep-seated landslide dam in the Siriu Reservoir (Curvature Carpathians, Romania). Landslides, 10(3), 323-329.

Mondini, A.C., Guzzetti, F., Reichenbach, P., Rossi, M., Cardinali, M., Ardizzone, F., 2011. Semi-automatic recognition and mapping of rainfall induced shallow landslides using optical satellite images. Remote Sensing of Environment, 115(7), 1743-1757.

Nefeslioglu, H.A., Duman, T.Y., Durmaz, S., 2008a. Landslide susceptibility mapping for a part of tectonic Kelkit Valley (Eastern Black Sea region of Turkey). Geomorphology, 94(3–4), 401-418.

Nefeslioglu, H.A., Gokceoglu, C., Sonmez, H., 2008b. An assessment on the use of logistic regression and artificial neural networks with different sampling strategies for the preparation of landslide susceptibility maps. Engineering Geology, 97(3–4), 171-191.

Neuhäuser, B., Terhorst, B., 2007. Landslide susceptibility assessment using “weights-of-evidence” applied to a study area at the Jurassic escarpment (SW-Germany). Geomorphology, 86(1–2), 12-24.

Ozdemir, A., 2011. Landslide susceptibility mapping using Bayesian approach in the Sultan Mountains (Akşehir, Turkey). Natural Hazards, 59(3), 1573-1607.

Ozdemir, A., Altural, T., 2013. A comparative study of frequency ratio, weights of evidence and logistic regression methods for landslide susceptibility mapping: Sultan Mountains, SW Turkey. Journal of Asian Earth Sciences, 64(0), 180-197.

Papathanassiou, G., Valkaniotis, S., Ganas, A., Pavlides, S., 2013. GIS-based statistical analysis of the spatial distribution of earthquake-induced landslides in the island of Lefkada, Ionian Islands, Greece. Landslides, 10(6), 771-783.

Pasuto, A., Silvano, S., Berlasso, G., 2000. Application Of Time Domain Reflectometry (Tdr) Technique In Monitoring The Pramollo Pass Landslide (Province Of Udine, Italy). In: E. Bromhead, N. Dixon, M.-L. Ibsen (Eds.), Landslides In Research, Theory And Practice. Thomas Telford Publishing, pp. 1189-1194.

PC-FVG, 2014. Protezione Civile Regione Autonoma Friuli-Venezia Giulia.

Petschko, H., Bell, R., Leopold, P., Heiss, G., Glade, T., 2013. Landslide Inventories for Reliable Susceptibility Maps in Lower Austria. In: C. Margottini, P. Canuti, K. Sassa (Eds.), Landslide Science and Practice. Springer Berlin Heidelberg, pp. 281-286.

Petschko, H., Brenning, A., Bell, R., Goetz, J., Glade, T., 2014. Assessing the quality of landslide susceptibility maps – case study Lower Austria. Nat. Hazards Earth Syst. Sci., 14(1), 95-118.

Piacentini, D., Troiani, F., Soldati, M., Notarnicola, C., Savelli, D., Schneiderbauer, S., Strada, C., 2012. Statistical analysis for assessing shallow-landslide susceptibility in South Tyrol (south-eastern Alps, Italy). Geomorphology, 151–152(0), 196-206.

Poli, S., Sterlacchini, S., 2007. Landslide Representation Strategies in Susceptibility Studies using Weights-of-Evidence Modeling Technique. Natural Resources Research, 16(2), 121-134.

Pradhan, B., 2011. An Assessment of the Use of an Advanced Neural Network Model with Five Different Training Strategies for the Preparation of Landslide Susceptibility Maps. Journal of Data Science, 9, 65-81.

Pradhan, B., Lee, S., Mansor, S., 2008. Application of a Data Mining Model and it's Cross Application for Landslide Hazard Analysis, A Case Study in Malaysia. Proceedings of COSPAR 2008, Montreal, Canada.

Qi, S., Xu, Q., Lan, H., Zhang, B., Liu, J., 2010. Spatial distribution analysis of landslides triggered by 2008.5.12 Wenchuan Earthquake, China. Engineering Geology, 116(1–2), 95-108.

Regmi, N., Giardino, J., McDonald, E., Vitek, J., 2013. A comparison of logistic regression-based models of susceptibility to landslides in western Colorado, USA. Landslides, 1-16.

Regmi, N.R., Giardino, J.R., Vitek, J.D., 2010. Modeling susceptibility to landslides using the weight of evidence approach: Western Colorado, USA. Geomorphology, 115(1–2), 172-187.

Remondo, J., González, A., De Terán, J., Cendrero, A., Fabbri, A., Chung, C.-J., 2003. Validation of Landslide Susceptibility Maps; Examples and Applications from a Case Study in Northern Spain. Natural Hazards, 30(3), 437-449.

San, B.T., 2014. An evaluation of SVM using polygon-based random sampling in landslide susceptibility mapping: The Candir catchment area (western Antalya, Turkey). International Journal of Applied Earth Observation and Geoinformation, 26(0), 399-412.

Sawatzky, D.L., Raines, G.L., Bonham-Carter, G.F., Looney, C.G., 2009. Spatial Data Modeller (SDM): ArcMAP 9.3 geoprocessing tools for spatial data modelling using weights of evidence, logistic regression, fuzzy logic and neural networks.

Schicker, R., Moon, V., 2012. Comparison of bivariate and multivariate statistical approaches in landslide susceptibility mapping at a regional scale. Geomorphology, 161–162(0), 40-57.

Simon, N., Crozier, M., de Róiste, M., Rafek, A.G., 2013. Point based assessment: Selecting the best way to represent landslide polygon as point frequency in landslide investigation. Electronic Journal of Geotechnical Engineering, 18 (D), 775-784.

Soeters, R., van Westen, C.J., 1996. Slope instability recognition, analysis, and zonation. In: A.K. Turner, R.L. Schuster (Eds.), Landslides: investigation and mitigation. Transportation Research Board, National Research Council. National Academy Press, Washington D.C., pp. 129-177.

Sterlacchini, S., Ballabio, C., Blahut, J., Masetti, M., Sorichetta, A., 2011. Spatial agreement of predicted patterns in landslide susceptibility maps. Geomorphology, 125(1), 51-61.

Süzen, M.L., Doyuran, V., 2004. Data driven bivariate landslide susceptibility assessment using geographical information systems: a method and application to Asarsuyu catchment, Turkey. Engineering Geology, 71(3–4), 303-321.

Thiery, Y., Malet, J.P., Sterlacchini, S., Puissant, A., Maquaire, O., 2007. Landslide susceptibility assessment by bivariate methods at large scales: Application to a complex mountainous environment. Geomorphology, 92(1–2), 38-59.

Tian, Y., XiaO, C., Liu, Y., Wu, L., 2008. Effects of raster resolution on landslide susceptibility mapping: A case study of Shenzhen. Science in China Series E: Technological Sciences, 51(2), 188-198.

Tropeano, D., Turconi, L., Sanna, S., 2004. Debris flows triggered by the 29 August 2003 cloudburst in Val Canale, eastern Italian Alps, Proceedings of the 10th Internationales Symposion InterPraevent 2004, Riva del Garda, Italy pp. 121-132.

Van Den Eeckhaut, M., Marre, A., Poesen, J., 2010. Comparison of two landslide susceptibility assessments in the Champagne–Ardenne region (France). Geomorphology, 115(1–2), 141-155.

Van Den Eeckhaut, M., Reichenbach, P., Guzzetti, F., Rossi, M., Poesen, J., 2009. Combined landslide inventory and susceptibility assessment based on different mapping units: an example from the Flemish Ardennes, Belgium. Nat. Hazards Earth Syst. Sci., 9(2), 507-521.

Van Den Eeckhaut, M., Vanwalleghem, T., Poesen, J., Govers, G., Verstraeten, G., Vandekerckhove, L., 2006. Prediction of landslide susceptibility using rare events logistic regression: A case-study in the Flemish Ardennes (Belgium). Geomorphology, 76(3–4), 392-410.

van Westen, C.J., 1993. Application of geographic information systems to landslide hazard zonationPh.D., ITC, Enschede, The Netherlands.

Van Westen, C.J., 2000. The Modelling Of Landslide Hazards Using Gis. Surveys in Geophysics, 21(2-3), 241-255.

van Westen, C.J., 2004. Geo - information tools for landslide risk assessment : an overview of recent development. In: W. Lacerda, M. Erlich, S.A.B. Fontoura, A.S.F. Sayao (Eds.), Landslides : evaluation and stabilization - glissement de terrain: Evaluation et Stabilisation : proceedings of the 9th international symposium on landslides, Rio de Janeiro, Brazil. Balkema, London, pp. 39-56.

van Westen, C.J., Castellanos, E., Kuriakose, S.L., 2008. Spatial data for landslide susceptibility, hazard, and vulnerability assessment: An overview. Engineering Geology, 102(3–4), 112-131.

van Westen, C.J., Rengers, N., Soeters, R., 2003. Use of Geomorphological Information in Indirect Landslide Susceptibility Assessment. Natural Hazards, 30(3), 399-419.

van Westen, C.J., Rengers, N., Terlien, M.T.J., Soeters, R., 1997. Prediction of the occurrence of slope instability phenomenal through GIS-based hazard zonation. Geologische Rundschau, 86(2), 404-414.

van Westen, C.J., Soeters, R., Sijmons, K., 2000. Digital geomorphological landslide hazard mapping of the Alpago area, Italy. International Journal of Applied Earth Observation and Geoinformation, 2(1), 51-60.

van Westen, C.J., van Asch, T.W.J., Soeters, R., 2006. Landslide hazard and risk zonation—why is it still so difficult? Bull Eng Geol Environ, 65(2), 167-184.

Varnes, D.J., Landslides, I.A.o.E.G.C.o., Slopes, O.M.M.o., 1984. Landslide hazard zonation: a review of principles and practice. Unesco.

von Ruette, J., Papritz, A., Lehmann, P., Rickli, C., Or, D., 2011. Spatial statistical modeling of shallow landslides—Validating predictions for different landslide inventories and rainfall events. Geomorphology, 133(1–2), 11-22.

Wang, H.B., Liu, G.J., Xu, W.Y., Wang, G.H., 2005. GIS-based landslide hazard assessment: an overview. Progress in Physical Geography, 29(4), 548-567.

Xu, C., Xu, X., Yao, X., Dai, F., 2013. Three (nearly) complete inventories of landslides triggered by the May 12, 2008 Wenchuan Mw 7.9 earthquake of China and their spatial distribution statistical analysis. Landslides, 1-21.

Yilmaz, I., 2010. The effect of the sampling strategies on the landslide susceptibility mapping by conditional probability and artificial neural networks. Environmental Earth Sciences, 60(3), 505-519.

Zumpano, V., Ciurean, R.L., Micu, M., Bãlteanu, D., Glade, T., 2013. Uncertainty associated with regional landslide risk analysis – a case study in Buzău County, Romania. Geophysical Research Abstracts, Vol. 15, EGU2013-9306

Zumpano, V., Hussin, H.Y., Reichenbach, P., Balteanu, D., Micu, M., Sterlacchini, S., 2014. A landslide susceptibility analysis for Buzău County, Romania. Romanian Journal of Geography/Revue Roumaine de Geographie, 58(1), 9-16.